AIMS Mathematics, 11(7): 21570–21606.
DOI: 10.3934/math.2026874
Received: 25 March 2026
Revised: 17 May 2026
Accepted: 20 May 2026
Published: 21 July 2026

http://www.aimspress.com/journal/Math

Research article

Mathematical modeling of human metapneumovirus transmission dynamics with optimal control analysis

Md Hossain Islam[1], Md. Nur Alam[2,3], Noor Muhammad[4], Xinsong Yang[1,*] and Md. Jakir Hossen[5,*]

[1] College of Electronics and Information Engineering, Sichuan University, Chengdu 610065, China
[2] School of Mathematical Sciences, Sunway University, Bandar Sunway, Petaling Jaya 47500, Selangor Darul Ehsan, Malaysia
[3] Department of Mathematics, Pabna University of Science and Technology, Pabna-6600, Bangladesh
[4] School of Mathematics, Sichuan University, Chengdu 610064, China
[5] Center for Advanced Analytics (CAA), COE for Artificial Intelligence, Faculty of Engineering and Technology (FET), Multimedia University, Melaka 75450, Malaysia

* **Correspondence:** Email: xinsongyang@scu.edu.cn, jakir.hossen@mmu.edu.my; Tel: 028-85463873; Fax: 028-85463873.

Abstract: Human metapneumovirus (HMPV) is a pathogen that causes severe respiratory infections, especially in children, the elderly, and immunocompromised people. Deterministic epidemiological models cannot capture memory effects or stochastic variability of the environment and thus limit the formulation of effective control measures. In this paper, we developed a stochastic optimal control problem, based on a fractional-order stochastic dynamic, to promote vaccination and treatment solutions to the disease burden. In this study, we designed a modified fractional-order stochastic SEIR model with a Brownian motion to consider long-range time memory effects and stochastic environmental variation. We verified the existence, uniqueness, and positivity of the model, as well as identified disease-free equilibrium, the basic reproduction number R_0, and endemic equilibrium. Local and global stability of both states were examined, and a bifurcation analysis disclosed a forward transcritical bifurcation at the point $R_0 = 1$. Sensitivity analysis highlighted the transmission rate β (+1.000), progression rate σ (+0.4545), and recovery rate γ (-0.6818) as critical parameters affecting R_0. We proposed an optimal control analysis that uncovered time-dependent optimal vaccination and treatment techniques. Under the optimal treatment-focused strategy, decreasing the fractional order α from 1.0 to 0.7 reduced peak infections by 36.1% (from 244 to 156 cases) and delayed the epidemic peak by 57.8% (from 26.8 to 42.3 days). A strong linear correlation ($R^2 = 0.96$) disclosed that lower fractional orders α impose earlier but less intensive interventions. This adaptive control framework offers the public health authorities a tool for designing an outbreak response that is resilient to real-life uncertainty.

Keywords: human metapneumovirus (HMPV); fractional stochastic SEIR model; reproduction number R_0; optimal control analysis; B-Spline collocation method; stability; bifurcation
Mathematics Subject Classification: 92D30, 34A08, 60H10, 34C23, 93E20

1. Introduction

Human metapneumovirus (HMPV) poses a significant disease burden on the global population, particularly affecting young children, elderly individuals, and immunocompromised persons. Since its first discovery in 2001, HMPV has been identified as a major etiologic agent of upper and lower respiratory tract infections, with seasonal outbreaks that cause significant morbidity and impose a considerable burden on healthcare infrastructures worldwide [1–3]. However, HMPV transmission dynamics through mathematical modeling have not been investigated as much, in comparison to the much larger amount of modeling information on other respiratory viruses like influenza and respiratory syncytial virus (RSV) [4, 5]. Nonetheless, mathematical modeling on HMPV transmission dynamics has not been quantitatively studied, especially compared to the vast amount of information modeling on other respiratory viruses like influenza and respiratory syncytial virus (RSV) that have been studied by mathematical models. The gap highlights a strong gap in the empirical and theoretical literature on the seasonal patterns of HMPV and the demographic risk patterns it induces. The traditional conceptual and methodological models used in the modeling literature of influenza and RSV do not provide enough conceptual and methodological frameworks to capture the unique epidemiological features of HMPV, such as age-specific attack rates and immune responses, which are necessary to predictive modeling [6]. HMPV has unique mathematical epidemiological issues that cannot be solved using standard deterministic models. The virus exhibits complicated patterns of transmission with high spatial heterogeneity, age-structured patterns of susceptibility, and high seasonal oscillations that differ by geographical region. Moreover, long-term immunity after the infection with HMPV is not fully defined, which also adds another ambiguity to the long-term predictions. Such epidemiological singularities demand the creation of specific modeling strategies that would be capable of handling the specific nature of the HMPV transmission behavior, as well as considering the high level of uncertainty that is inherent in estimating parameters and disease developmental patterns [7]. Fractional calculus provides an effective mathematical model to improve the biological credibility of epidemiological models by including memory effects and non-local interactions, especially when it comes to respiratory viruses with complicated incubation and immunity mechanisms [8, 9]. Compared to integer-order derivatives, which may be based on Markovian dynamics, the historical dependence of disease transmission in a fractional derivative offers a more subtle understanding of the effect of past states on contemporary transmission rates. Such mathematical formalism is consistent with the known requirement to have models more representative of the temporal dependence in data on epidemics in the real world, where present-day rates of infection are inherently related to past contact processes and immunity conditions. Stochastic modeling is another important development in epidemiological modeling, as it offers a solution to the drawbacks of purely deterministic modeling. Moreover, the transmission of diseases in the real world is mainly determined by millions of accidents such as changes in human behavior, the environment, and the reactions of healthcare systems. Stochastic

differential equations offer a logical mathematical vocabulary to include such uncertainties, and models can produce probabilistic forecasts rather than single trajectory forecasts [10]. This probabilistic model is particularly beneficial in the context of the public health planning process, because it enables one to quantify risks and construct effective intervention strategies that can be applicable in different epidemic situations. Building and modeling epidemiology makes it possible to replicate the transmission of pathogens, quantify the possible effect of different control interventions, and predict the future epidemiology of future outbreaks. The Susceptible-Exposed-Infectious-Recovered (SEIR) compartmental model remains popular in the field, and the transitions are modeled using ordinary differential equations, dividing the population by compartment [11, 12]. This simplification is useful in the general trend analysis but not in the representation of the discrete, context-specific fluctuations in actual epidemiological conditions, including demographic, climate change, and non-regular behavior choices of individuals and organizations, over time, as well as distributions of events [13, 14]. The most significant of these are the stochastic effects, when the context is spatially concentrated, or when the overall process involves random perturbation, where similar sets of stochastic basic reproductive numbers may produce significantly different cumulative incidence curves. Therefore, although deterministic SEIR models are powerful aids in the process of overall strategic planning, they cannot effectively represent the probabilistic, path-dependent aspects of disease spread that are critical to sound prediction and the formulation of efficient intervention plans [15]. To overcome the above restrictions, stochastic modeling has been implemented as a probabilistic extension of the conventional SEIR model [16]. Since they incorporate random variables, stochastic models better capture all the uncertainty in the transmission of pathogens, thus giving a more precise description of epidemic behavior. Stochastic differential equations are equations that include these random perturbations to every compartmental state using Brownian motion or Wiener processes [17–19]. In this study, we include the bifurcation analysis to investigate the underlying change in the dynamics of the disease that takes place when the basic reproduction number passes the critical value of the disease named the critical value of reproduction as the value of one of the basic reproduction numbers, $\mathcal{R}_0 = 1$, the value of one divergence, denoted by R. In this analysis, a forward trans-critical bifurcation is determined, which marks the destabilization of the disease-free equilibrium and the simultaneous appearance of an endemic equilibrium. This dichotomy framework is important in determining the effectiveness of intervention measures because it defines the circumstances in which the disease can be eliminated or maintained at the endemic level. The optimal control theory provides the mathematical foundations of the design of the intervention approaches that will maximize the overall benefits to the population and simultaneously consider the resource constraints and the implementation costs. Within HMPV, where there is a range of intervention modalities, such as vaccination programs, antiviral services, and non-pharmaceutical strategies, the best control strategies can be used to define the most effective use of limited resources within time frames [20]. With the formulation of public health decision-making as a formal optimization problem [21], it will be possible to develop dynamically adaptive intervention policies that adapt to changing epidemic conditions, which may potentially outperform the strategies that are stationary. The implementation of a strong numerical framework based on a direct B-spline collocation method that simultaneously separates state and control variables using smooth spline basis functions to address the complexity of fractional stochastic epidemic models has been proposed [22, 23]. This enables precise computation of fractional derivatives, effective handling of stochastic terms, and direct solution of the resulting nonlinear programming problem for optimal

control design. The contributions of this paper are as follows:

- We develop a fractional-order stochastic SEIR model for HMPV that incorporates memory effects and environmental variability. We establish the model's mathematical foundations by proving solution existence, uniqueness, and positivity. The disease-free and endemic equilibria are determined along with the basic reproduction number $\mathcal{R}_0$. Stability analysis characterizes the equilibrium behavior, while bifurcation analysis reveals a forward transcritical bifurcation at $\mathcal{R}_0 = 1$, establishing threshold conditions for disease persistence. Sensitivity analysis identifies the transmission rate β, progression rate σ, and recovery rate γ as the most influential parameters for disease transmission dynamics.
- We formulate an optimal control problem to derive time-dependent vaccination and treatment strategies that minimize the disease burden under stochastic perturbations. Numerical solutions obtained via a B-spline collocation method [24–27] demonstrate that a treatment-focused strategy reduces peak infections by 36.1% and delays the epidemic peak by 57.8% as fractional order α decreases. Moreover, the fractional order and the best time to implement the intervention are positively correlated (the value of R^2 is 0.96), which implies that a lower fractional order requires earlier but less intensive interventions.
- We use the B-spline collection method for key reduction of this virus. This method enhances the simulation and optimization of interventions under uncertainty, contributing to advancements in stochastic disease modeling and optimal control.

The structure of this manuscript is as follows: We introduce the necessary preliminaries and mathematical tools in Section 2. Section 3 contains the development of a fractional-order stochastic SEIR model of HMPV and its base properties. In Section 4, we provide an analytical study of the model, including equilibrium points and the basic reproduction number. In Section 5, we study the bifurcation at the critical threshold. Section 6 contains a sensitivity analysis to identify the salient parameters. In Section 7, there is a definition of the optimal control problem, and we present the relevant numerical results. Last, in Section 8, we present the conclusion and outline future research prospective directions.

2. Preliminaries

Mathematical constructs are developed based on the foundations of mathematics, with the addition of a tool of fractional calculus to model the effects of memory, a stochastic process to model the variability of the environment, and the use of optimal control to design the intervention. Strict analytical statements certifying the existence, uniqueness, and positivity of solutions provide the essential background required for the latter formulation and analysis.

All stochastic processes considered in this work are defined on a complete probability space $(\Omega, \mathcal{F}, \{\mathcal{F}_t\}_{t\geq 0}, \mathbb{P})$ satisfying the usual conditions. The noise terms dW_S, dW_E, dW_I, and dW_R denote the differentials of mutually independent standard Wiener processes. This choice reflects uncorrelated environmental fluctuations affecting each compartment independently.

Definition 2.1. For $\alpha \in (0, 1)$, the Caputo fractional derivative of $x(t)$ is:

$$ {}_C D_t^{\alpha} x(t) = \frac{1}{\Gamma(1-\alpha)} \int_0^t (t-s)^{-\alpha} x'(s)\, ds. $$

In the stochastic fractional differential equations of this work, the notation $D_t^\alpha X(t) = f(t, X)dt + g(t, X)dW(t)$ is understood as the equivalent integral equation

$$X(t) = X(0) + \frac{1}{\Gamma(\alpha)} \int_0^t (t-s)^{\alpha-1} f(s, X(s))\, ds + \frac{1}{\Gamma(\alpha)} \int_0^t (t-s)^{\alpha-1} g(s, X(s))\, dW(s),$$

where the first integral is the Riemann–Liouville fractional integral of the drift, and the second is an Itô integral with a fractional kernel. This interpretation ensures consistency between the Caputo derivative and the stochastic driving process [28].

Proposition 2.1. For the stochastic fractional-order SEIR model,

$${}_C D_t^\alpha X(t) = F(t, X(t)) + G(t, X(t))\, dB^H(t).$$

With Lipschitz continuous coefficients and initial condition $X(0) = X_0 \in \mathbb{R}_+^4$, there exists a unique global positive solution $X(t) \in \mathbb{R}_+^4$ for all $t \geq 0$.

Lemma 2.1. If initial conditions satisfy $S(0), E(0), I(0), R(0) > 0$, then the solution remains positive almost surely.

$$\mathbb{P}\{S(t) > 0, E(t) > 0, I(t) > 0, R(t) > 0 \text{ for all } t \geq 0\} = 1.$$

3. Model formulation

We begin with a generalization of the classical SEIR compartmental model to the use of fractional-order derivatives [29, 30]. The population is broken down into four epidemiological compartments, including susceptible (S), exposed (E), infectious (I), and recovered (R), as shown in Figure 1. The fundamental model is Caputo fractional derivatives of order $\alpha \in (0, 1]$ and contains multiplicative noises, yielding the following system:

$$\begin{cases} D_t^\alpha S = \left(\mu N - \beta \dfrac{SI}{N} - \mu S\right) dt + \sigma_S S\, dW_S, \\ D_t^\alpha E = \left(\beta \dfrac{SI}{N} - (\sigma + \mu)E\right) dt + \sigma_E E\, dW_E, \\ D_t^\alpha I = (\sigma E - (\gamma + \mu)I)\, dt + \sigma_I I\, dW_I, \\ D_t^\alpha R = (\gamma I - \mu R)\, dt + \sigma_R R\, dW_R, \end{cases} \tag{1}$$

where the Caputo fractional derivative operator is represented by D_t^α. Transmission, progression, recovery, and mortality rates are represented by parameters β, σ, γ, and μ, respectively. Independent Wiener processes $\{W_S, W_E, W_I, W_R\}$ with matching diffusion coefficients $\{\sigma_S, \sigma_E, \sigma_I, \sigma_R\}$ are used to model.

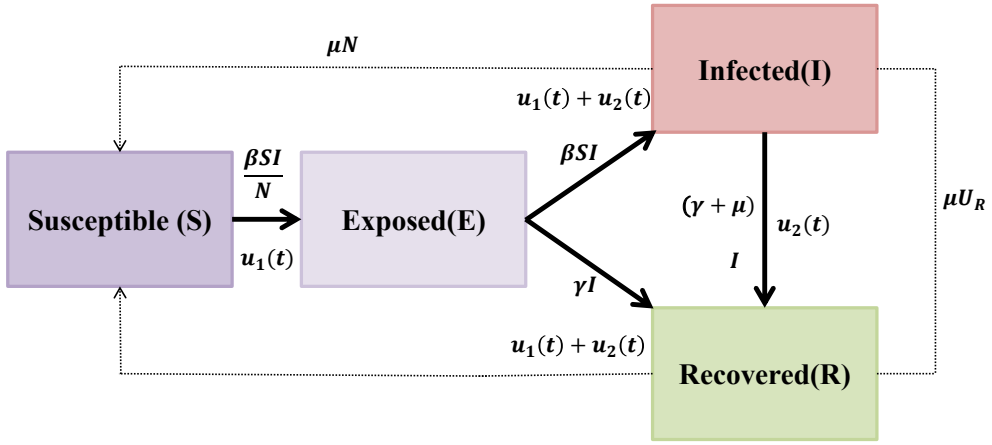

Figure 1. Schematic representation of the SEIR compartmental model for HMPV.

We introduce the force of infection $\lambda(t)$ and aggregate important parameter combinations to improve analytical clarity and ease further mathematical analysis. The force of infection, representing the instantaneous risk of infection for susceptible individuals, is defined as $\lambda(t) = \frac{\beta I(t)}{N}$.

For notational simplicity, we define the following compound parameters: $\theta_E = \sigma + \mu, \quad \theta_I = \gamma + \mu.$

$$\begin{cases} D_t^\alpha S(t) = \mu N - \lambda(t)S(t) - \mu S(t) + \sigma_S S(t)\, dW_S(t), \\ D_t^\alpha E(t) = \lambda(t)S(t) - \theta_E E(t) + \sigma_E E(t)\, dW_E(t), \\ D_t^\alpha I(t) = \sigma E(t) - \theta_I I(t) + \sigma_I I(t)\, dW_I(t), \\ D_t^\alpha R(t) = \gamma I(t) - \mu R(t) + \sigma_R R(t)\, dW_R(t). \end{cases} \tag{2}$$

Fractional order α governs the memory intensity within the system, with $\alpha = 1$ recovering the classical integer-order case. Each compartment's uncorrelated environmental changes are modeled by distinct Wiener processes. The multiplicative form $\sigma_j X_j(t) dW_j(t)$ is chosen because random fluctuations in population compartments scale naturally with the size of the affected subpopulation. Larger groups experience proportionally larger absolute variability, while the diffusion vanishes as a compartment empties, preserving the non-negativity of solutions. The independence of the Wiener processes across compartments reflects the assumption that environmental perturbations act on each epidemiological state without strong cross-correlation. The model (2) is analyzed under epidemiologically consistent non-negative initial conditions.

$$S(0) = S_0 \geq 0, \quad E(0) = E_0 \geq 0, \quad I(0) = I_0 \geq 0, \quad R(0) = R_0 \geq 0,$$

with $S_0 + E_0 + I_0 + R_0 = N$, where N represents the constant total population size.

Table 1 presents a summary of the epidemiological and mathematical parameters that control the fractional stochastic SEIR model. The parameters are biologically defined, and the ranges of values of each parameter with the corresponding references are clearly given. The fractional stochastic

SEIR model (2) is a mathematical model of HMPV transmission dynamics. Infected people affect the susceptible through contact with infectious individuals at a rate of $\lambda(t) = \beta I(t)/N$ infections per person of contact, thus transferring one to the exposed compartment. Exposed individuals will become infectious after an average duration of $1/\sigma$ days following their exposure. The rate of infection is γ, so infected individuals obtain temporary immunity. Contact behavior, diagnostic accuracy, and environmental uncertainties are represented by the inclusion of Caputo fractional derivatives and stochastic terms, respectively. Such an integrated framework has the benefit of providing improved predictive power as compared to standard deterministic models, especially with pathogens that display complex temporal behavior such as HMPV.

Table 1. Epidemiological parameters for the fractional stochastic SEIR model of HMPV transmission.

Parameter	Biological Description	Value/Range	Source
β	Effective contact rate between infectious and susceptible individuals	0.15 – 0.45 day^{-1}	[31]
σ	Progression rate from exposed to infectious state (inverse of average latency period)	0.125 – 0.25 day^{-1} (4-8 days latency)	[32]
μ	Natural mortality and birth rate (per capita)	3.9×10^{-5} day^{-1}	[33]
γ	Recovery rate from infectious to recovered state (inverse of average infectious period)	$0.1 - 0.2\ \text{day}^{-1}$ (5-10 days infectious)	[33]
α	Fractional order governing memory effects	0.7 – 1.0 (dimensionless)	[33]
σ_S	Diffusion coefficient for environmental stochasticity in susceptible compartment	0.01 – 0.05 (dimensionless)	[34]
σ_E	Diffusion coefficient for environmental stochasticity in exposed compartment	0.01 – 0.05 (dimensionless)	[35]
σ_I	Diffusion coefficient for environmental stochasticity in infectious compartment	0.02 – 0.08 (dimensionless)	[35]
σ_R	Diffusion coefficient for environmental stochasticity in recovered compartment	0.01 – 0.04 (dimensionless)	[35]

3.1. Basic properties of the model

In this section, we establish the fundamental mathematical properties of the fractional stochastic SEIR system (2), ensuring its well-posedness for epidemiological analysis. We prove the existence,

uniqueness, positivity, and boundedness of solutions under biologically relevant conditions.

3.2. Positivity of solutions

Lemma 3.1. If the initial conditions satisfy $S(0) > 0$, $E(0) \geq 0$, $I(0) \geq 0$, $R(0) \geq 0$, then for all $t > 0$, the solutions of (2) satisfy almost surely.

$$S(t) > 0, \quad E(t) \geq 0, \quad I(t) \geq 0, \quad R(t) \geq 0.$$

Moreover, if $E(0) + I(0) > 0$, then $S(t) > 0$, $E(t) > 0$, $I(t) > 0$, and $R(t) > 0$ for all $t > 0$.

Proof. We prove the stronger positivity result using stochastic analysis techniques.

Susceptible compartment $S(t)$ satisfies,

$$D_t^\alpha S(t) \geq -(\lambda(t) + \mu)S(t) + \sigma_S S(t)\, dW_S(t).$$

By the fractional Itô formula for Caputo fractional stochastic differential equations [28], the differential of $\log S(t)$ satisfies

$$D_t^\alpha \log S(t) \geq -(\lambda(t) + \mu) - \frac{1}{2}\sigma_S^2 + \sigma_S dW_S(t).$$

$$D_t^\alpha \log S(t) \geq -(\lambda(t) + \mu) - \frac{1}{2}\sigma_S^2 + \sigma_S\, dW_S(t).$$

Integrating from 0 to t.

$$S(t) \geq S(0) \exp\left(- \int_0^t (\lambda(s) + \mu)\, d^\alpha s - \frac{1}{2}\sigma_S^2 t^\alpha + \sigma_S W_S^\alpha(t) \right) > 0.$$

When $E(0) \geq 0$, consider the representation

$$E(t) = E(0)E_\alpha(-\theta_E t^\alpha) + \int_0^t (t-s)^{\alpha-1} E_{\alpha,\alpha}(-\theta_E(t-s)^\alpha)\lambda(s)S(s)\, d^\alpha s.$$

Both terms are non-negative since $\lambda(s)S(s) \geq 0$ and the Mittag–Leffler functions E_α and $E_{\alpha,\alpha}$ are completely monotonic for $\alpha \in (0, 1]$. If $E(0) > 0$ or $\lambda(s)S(s) > 0$ for some s, then $E(t) > 0$. Similarly, for an infectious compartment,

$$I(t) = I(0)E_\alpha(-\theta_I t^\alpha) + \sigma \int_0^t (t-s)^{\alpha-1} E_{\alpha,\alpha}(-\theta_I(t-s)^\alpha)E(s)\, d^\alpha s \geq 0.$$

Positivity follows from $E(s) \geq 0$.

For a recovered compartment we get,

$$R(t) = R(0)E_\alpha(-\mu t^\alpha) + \gamma \int_0^t (t-s)^{\alpha-1} E_{\alpha,\alpha}(-\mu(t-s)^\alpha)I(s)\, d^\alpha s \geq 0.$$

Thus, all compartments maintain non-negativity, and under initial infection ($E(0) + I(0) > 0$), strict positivity holds for all $t > 0$. □

3.3. Boundedness and invariant region

Theorem 3.1. The solutions of (2) are uniformly bounded almost surely and satisfy $\mathbb{E}[S(t)+E(t)+I(t)+R(t)] = N$ for all $t \geq 0$. The biologically feasible region $\Omega = \{(S, E, I, R) \in \mathbb{R}^4_+ : \mathbb{E}[S + E + I + R] = N\}$ is positively invariant under the expectation operator, and the total population remains almost surely bounded.

Proof. Define the total population $N(t) = S(t) + E(t) + I(t) + R(t)$. Summing all equations of (2) yields

$$D_t^\alpha N(t) = \mu N - \mu N(t) + \sum_{j\in\{S,E,I,R\}} \sigma_j X_j(t) dW_j(t).$$

Taking expectations on both sides and using the martingale property of the Itô integral gives

$$D_t^\alpha \mathbb{E}[N(t)] = \mu N - \mu \mathbb{E}[N(t)].$$

This fractional differential equation for $m(t) = \mathbb{E}[N(t)]$ has the solution

$$m(t) = N - (N - m(0))E_\alpha(-\mu t^\alpha),$$

where E_α is the Mittag–Leffler function. Since $0 < E_\alpha(-\mu t^\alpha) \leq 1$ for $t \geq 0$, we obtain $\min(N, m(0)) \leq m(t) \leq \max(N, m(0))$. In particular, if $m(0) = N$, then $\mathbb{E}[N(t)] = N$ for all $t \geq 0$, establishing invariance of the expected total population. For almost sure boundedness, apply the fractional Itô formula to $V(N) = N^2$.

$$D_t^\alpha V(N(t)) \leq 2N(t) D_t^\alpha N(t) + \sum_j \sigma_j^2 X_j^2(t) \leq 2\mu N^2 - 2\mu N^2(t) + \bar{\sigma}^2 N^2(t),$$

where $\bar{\sigma}^2 = \max\{\sigma_S^2, \sigma_E^2, \sigma_I^2, \sigma_R^2\}$. For $\mu > \bar{\sigma}^2/2$, we have

$$D_t^\alpha \mathbb{E}[V(N(t))] \leq 2\mu N^2 - (2\mu - \bar{\sigma}^2)\mathbb{E}[N^2(t)].$$

By fractional comparison principles, $\mathbb{E}[N^2(t)]$ remains bounded, and via Chebyshev's inequality, $N(t)$ is almost surely uniformly bounded.

4. Model analysis

The analytical results presented in this section pertain to the deterministic skeleton of the stochastic fractional model (2), obtained by setting the diffusion coefficients $\sigma_S, \sigma_E, \sigma_I, \sigma_R$ to zero. The equilibrium points, basic reproduction number, and stability conditions are derived in this deterministic framework. Their relevance to the full stochastic model is as follows: The disease-free equilibrium corresponds to almost sure extinction of the infection when $\mathcal{R}_0 < 1$, and the endemic equilibrium characterizes the mean behavior of the stationary distribution when $\mathcal{R}_0 > 1$ and the noise intensities remain moderate. In the full stochastic fractional model, $\mathcal{E}_0$ is not a fixed point in the pathwise sense but rather an absorbing sstate; once the infection compartments reach zero, they remain zero almost surely. The endemic equilibrium $\mathcal{E}^*$ corresponds to the mean of the stationary distribution toward which the process converges when $\mathcal{R}_0 > 1$ and the noise intensities remain moderate. Sample paths fluctuate persistently around this mean due to the continuous action of the Wiener processes.

4.1. Disease-free equilibrium

For the fractional stochastic SEIR system (2), a disease-free equilibrium (DFE) represents a steady state where the infection is not present in the population. This corresponds to the conditions $E(t) = 0$ and $I(t) = 0$ for all $t \geq 0$. To find the DFE, we consider the deterministic skeleton of the model by setting the stochastic terms to zero and solving the equilibrium equations $D_t^\alpha X = 0$:

$$\begin{cases} 0 = \mu N - \mu S^*, \\ 0 = -(\sigma + \mu)E^*, \\ 0 = \sigma E^* - (\gamma + \mu)I^*, \\ 0 = \gamma I^* - \mu R^*. \end{cases} \tag{3}$$

Under the infection-free assumption $E^* = 0$ and $I^* = 0$, the system simplifies to:

$$0 = \mu N - \mu S^* \quad \Rightarrow \quad S^* = N, \qquad 0 = -\mu R^* \quad \Rightarrow \quad R^* = 0.$$

Thus, the unique deterministic disease-free equilibrium is

$$\mathcal{E}_0 = (S^*, E^*, I^*, R^*) = (N, 0, 0, 0). \tag{4}$$

For the full stochastic model (2), the concept of a fixed point must be interpreted in a mean-square sense. At $\mathcal{E}_0$, the diffusion matrix $G(X) = \mathrm{diag}(\sigma_S S, \sigma_E E, \sigma_I I, \sigma_R R)$ evaluates to

$$G(\mathcal{E}_0) = \mathrm{diag}(\sigma_S N, 0, 0, 0).$$

This indicates that stochastic perturbations vanish in the E, I, and R compartments at the DFE, leaving only demographic noise in the susceptible compartment. Consequently, $\mathcal{E}_0$ is a degenerate stochastic equilibrium. Its stability must therefore be analyzed through linearization and spectral analysis of the associated fractional Jacobian operator.

4.2. Local stability of disease-free equilibrium

Theorem 4.1. For the deterministic fractional skeleton of model (2), with Caputo derivative of order $\alpha \in (0, 1]$, the disease-free equilibrium $\mathcal{E}_0 = (N, 0, 0, 0)$ is locally asymptotically stable if $\mathcal{R}_0 < 1$, and unstable if $\mathcal{R}_0 > 1$.

Proof. Consider the linearization of model (2) around $\mathcal{E}_0$. The Jacobian matrix evaluated at $\mathcal{E}_0$ is

$$J(\mathcal{E}_0) = \begin{bmatrix} -\mu & 0 & -\beta & 0 \\ 0 & -(\sigma + \mu) & \beta & 0 \\ 0 & \sigma & -(\gamma + \mu) & 0 \\ 0 & 0 & \gamma & -\mu \end{bmatrix}.$$

The characteristic equation is

$$\det(J - \lambda I) = (\lambda + \mu)^2 \left[\lambda^2 + (\sigma + \gamma + 2\mu)\lambda + (\sigma + \mu)(\gamma + \mu) - \beta\sigma\right] = 0. \tag{5}$$

This yields eigenvalues $\lambda_{1,2} = -\mu$ (with multiplicity 2) and the roots of the quadratic.

$$\lambda^2 + a\lambda + b = 0, \tag{6}$$

where $a = \sigma + \gamma + 2\mu > 0$ and $b = (\sigma + \mu)(\gamma + \mu) - \beta\sigma$. Using $\mathcal{R}_0 = \frac{\beta\sigma}{(\sigma+\mu)(\gamma+\mu)}$, we rewrite b as,

$$b = (\sigma + \mu)(\gamma + \mu)(1 - \mathcal{R}_0). \tag{7}$$

For $\mathcal{R}_0 < 1$, we have $b > 0$ and $a > 0$. The Routh-Hurwitz conditions for are satisfied.

$$a > 0 \quad \text{and} \quad b > 0.$$

Thus, all eigenvalues of have negative real parts. For fractional-order systems with Caputo derivative of order α, the stability condition requires $|\arg(\lambda_i)| > \alpha\pi/2$ for all eigenvalues λ_i [36]. Since all eigenvalues have negative real parts when $\mathcal{R}_0 < 1$, this condition is satisfied. When $\mathcal{R}_0 > 1$, $b < 0$, implying at least one eigenvalue with a positive real part, making $\mathcal{E}_0$ unstable. □

4.3. Global stability of disease-free equilibrium

Theorem 4.2. For the deterministic fractional skeleton of model (2) with $\mathcal{R}_0 < 1$, the disease-free equilibrium $\mathcal{E}_0$ is globally asymptotically stable in the biologically feasible region $\Omega = \{(S, E, I, R) \in \mathbb{R}^4_+ : S + E + I + R = N\}$.

Proof. Consider the Lyapunov function candidate is

$$V(E, I) = E + \frac{\sigma + \mu}{\sigma} I. \tag{8}$$

Applying the Caputo fractional derivative:

$$\begin{aligned} D_t^\alpha V &= D_t^\alpha E + \frac{\sigma + \mu}{\sigma} D_t^\alpha I \\ &= \left[\beta \frac{SI}{N} - (\sigma + \mu)E\right] + \frac{\sigma + \mu}{\sigma} \left[\sigma E - (\gamma + \mu)I\right] \\ &= \beta \frac{SI}{N} - \frac{(\sigma + \mu)(\gamma + \mu)}{\sigma} I. \end{aligned} \tag{9}$$

Since $S \leq N$ in Ω, we have $\frac{S}{N} \leq 1$, thus,

$$D_t^\alpha V \leq \beta I - \frac{(\sigma + \mu)(\gamma + \mu)}{\sigma} I = \frac{(\sigma + \mu)(\gamma + \mu)}{\sigma} (\mathcal{R}_0 - 1) I. \tag{10}$$

When $\mathcal{R}_0 < 1$, $D_t^\alpha V \leq 0$ for all $(E, I) \in \Omega$, with equality only when $I = 0$. Let $M = \{(S, E, I, R) \in \Omega : D_t^\alpha V = 0\}$. In M, $I = 0$, and from (2) we get

$$D_t^\alpha I = \sigma E - (\gamma + \mu)I = \sigma E. \tag{11}$$

Since $D_t^\alpha I = 0$ in M, we have $\sigma E = 0 \Rightarrow E = 0$. The largest invariant set in M is $\mathcal{E}_0 = (N, 0, 0, 0)$. By the fractional LaSalle invariance principle [37], all solutions converge to $\mathcal{E}_0$ as $t \to \infty$.

Thus, $\mathcal{E}_0$ is globally asymptotically stable in Ω when $\mathcal{R}_0 < 1$. □

Remark 4.1. The stability analysis reveals that the disease-free equilibrium $\mathcal{E}_0$ is locally asymptotically stable when $\mathcal{R}_0 < 1$ and unstable when $\mathcal{R}_0 > 1$. Moreover, the Lyapunov function approach establishes global asymptotic stability of $\mathcal{E}_0$ in the biologically feasible region for $\mathcal{R}_0 < 1$, ensuring complete disease elimination from any initial state.

4.4. Basic reproduction number

The basic reproduction number, denoted $\mathcal{R}_0$, is a fundamental epidemiological threshold that quantifies the expected number of secondary infections generated by a single infectious individual introduced into a fully susceptible population. This critical parameter determines whether a disease will invade a population ($\mathcal{R}_0 > 1$) or fade out ($\mathcal{R}_0 < 1$).

We derive $\mathcal{R}_0$ for the fractional-order stochastic SEIR model (2) using the next generation matrix approach [38, 39]. Considering the deterministic counterpart (noise terms excluded) and focusing on the infected compartments (E, I), we define $\mathbf{x} = [E, I]^\top$, which is linearized at the disease-free equilibrium $\mathcal{E}_0 = (N, 0, 0, 0)$; we decompose the transmission dynamics into new infections and transitions between infected states.

$$D_t^\alpha \mathbf{x} = \mathcal{F}(\mathbf{x}) - \mathcal{V}(\mathbf{x}),$$

where the infection vector $\mathcal{F}$ and transition vector $\mathcal{V}$ are given by,

$$\mathcal{F}(\mathbf{x}) = \begin{bmatrix} \beta \dfrac{SI}{N} \\ 0 \end{bmatrix}, \qquad \mathcal{V}(\mathbf{x}) = \begin{bmatrix} (\sigma + \mu)E \\ -\sigma E + (\gamma + \mu)I \end{bmatrix}.$$

The Jacobian matrices evaluated at $\mathcal{E}_0$ are.

$$F = \left.\frac{\partial \mathcal{F}}{\partial \mathbf{x}}\right|_{\mathcal{E}_0} = \begin{bmatrix} 0 & \beta \\ 0 & 0 \end{bmatrix}, \qquad V = \left.\frac{\partial \mathcal{V}}{\partial \mathbf{x}}\right|_{\mathcal{E}_0} = \begin{bmatrix} \sigma + \mu & 0 \\ -\sigma & \gamma + \mu \end{bmatrix}.$$

The next-generation matrix is $K = FV^{-1}$, where

$$V^{-1} = \frac{1}{(\sigma + \mu)(\gamma + \mu)} \begin{bmatrix} \gamma + \mu & 0 \\ \sigma & \sigma + \mu \end{bmatrix}. \tag{12}$$

$$K = \frac{1}{(\sigma + \mu)(\gamma + \mu)} \begin{bmatrix} \beta\sigma & \beta(\sigma + \mu) \\ 0 & 0 \end{bmatrix}. \tag{13}$$

The basic reproduction number is the spectral radius (dominant eigenvalue) of K.

$$\mathcal{R}_0 = \rho(K) = \frac{\beta\sigma}{(\sigma + \mu)(\gamma + \mu)}. \tag{14}$$

Remark 4.2. The expression for $\mathcal{R}_0$ in (14) coincides with the classical integer-order SEIR model and is independent of the fractional order α and the stochastic diffusion coefficients $\sigma_S, \sigma_E, \sigma_I, \sigma_R$. This occurs because $\mathcal{R}_0$ is derived from the linearized deterministic infection subsystem at equilibrium, and the fractional order does not alter the equilibrium conditions or the linearization of new infection terms [40]. For the stochastic model, $\mathcal{R}_0$ serves as a threshold in expectation; however, the actual dynamics are influenced by memory effects (governed by α) and environmental noise. In the following sections, we use $\mathcal{R}_0$ as a reference threshold while analyzing the impact of fractional order and stochasticity on system behavior.

Remark 4.3. In the stochastic fractional model, $\mathcal{R}_0$ serves as a threshold in expectation and probability. When $\mathcal{R}_0 < 1$, the infection dies out almost surely. When $\mathcal{R}_0 > 1$, the disease persists with positive probability, and the state converges to a stationary distribution centered near the deterministic endemic equilibrium, provided the noise intensities are not excessively large. Fractional order α does not affect the algebraic value of $\mathcal{R}_0$ but governs the memory-dependent transient behavior and the speed of convergence to the stationary regime.

4.5. Endemic equilibrium analysis

An endemic equilibrium (EE) of (2) corresponds to a state where the disease persists at a constant positive level. We establish conditions for the existence and uniqueness of such an equilibrium.

Theorem 4.3. The fractional stochastic SEIR (2) model admits a unique positive endemic equilibrium $E^* = (S^*, E^*, I^*, R^*)$ if and only if $R_0 > 1$. The equilibrium components are given by:

$$S^* = \frac{N}{\mathcal{R}_0}, \tag{15}$$

$$E^* = \frac{\gamma + \mu}{\sigma} I^*, \tag{16}$$

$$I^* = \frac{\mu N}{\beta}(\mathcal{R}_0 - 1), \tag{17}$$

$$R^* = \frac{\gamma}{\mu} I^*. \tag{18}$$

Proof. To find the endemic equilibrium, we consider the deterministic skeleton of system (2) by setting the stochastic terms to zero and requiring all Caputo derivatives to vanish.

$$\begin{cases} 0 = \mu N - \beta \frac{S^* I^*}{N} - \mu S^*, & \text{(a)} \\ 0 = \beta \frac{S^* I^*}{N} - (\sigma + \mu) E^*, & \text{(b)} \\ 0 = \sigma E^* - (\gamma + \mu) I^*, & \text{(c)} \\ 0 = \gamma I^* - \mu R^*. & \text{(d)} \end{cases}$$

From (c), we obtain,

$$E^* = \frac{\gamma + \mu}{\sigma} I^*.$$

From (d),

$$R^* = \frac{\gamma}{\mu} I^*.$$

Substituting E^* into (b) gives

$$\beta \frac{S^* I^*}{N} = (\sigma + \mu) \frac{\gamma + \mu}{\sigma} I^*.$$

Assuming $I^* > 0$ (endemic state), we solve for S^*

$$S^* = \frac{N(\sigma + \mu)(\gamma + \mu)}{\beta \sigma} = \frac{N}{\mathcal{R}_0},$$

where we recognize $\mathcal{R}_0 = \frac{\beta\sigma}{(\sigma+\mu)(\gamma+\mu)}$, Substituting S^* into (a),

$$\mu N = \beta \frac{N}{\mathcal{R}_0} \frac{I^*}{N} + \mu \frac{N}{\mathcal{R}_0} = \frac{\beta}{\mathcal{R}_0} I^* + \frac{\mu N}{\mathcal{R}_0}.$$

Rearranging and solving for I^*,

$$I^* = \frac{\mu N}{\beta}(\mathcal{R}_0 - 1).$$

For biological relevance, we require $I^* > 0$, which holds if and only if $\mathcal{R}_0 > 1$. When $\mathcal{R}_0 \leq 1$, Eq (17) yields $I^* \leq 0$, which does not correspond to an endemic state. The expressions for E^* and R^* follow directly from (16) and (18). Thus, a unique positive endemic equilibrium exists precisely when $\mathcal{R}_0 > 1$. □

Remark 4.4. The equilibrium points $\mathcal{E}_0$ and $\mathcal{E}^*$ are derived from the deterministic skeleton and can be interpreted with the full stochastic setting. In the stochastic fractional model, $\mathcal{E}_0$ represents the absorbing disease-free state where $E = I = 0$ almost surely. The endemic equilibrium $\mathcal{E}^*$ corresponds to the expected value of the stationary distribution that the process converges to when $\mathcal{R}_0 > 1$ and the diffusion coefficients are not excessively large. This interpretation aligns with the stability results of Section 4, which are framed in terms of convergence in expectation and almost sure extinction.

Remark 4.5. The basic reproduction number $\mathcal{R}_0$ is derived from the deterministic skeleton of the model and therefore does not depend on fractional order α or the diffusion coefficients. In the full stochastic fractional system, $\mathcal{R}_0$ retains its role as a threshold but only in a probabilistic sense. When $\mathcal{R}_0 < 1$, the infection dies out almost surely, regardless of initial conditions. When $\mathcal{R}_0 > 1$, the disease persists with positive probability and the process converges to a stationary distribution whose mean is centered near the deterministic endemic equilibrium $\mathcal{E}^*$, provided the noise intensities are not so large as to drive the infection to extinction through random fluctuations. Fractional order α does not alter the algebraic value of $\mathcal{R}_0$ but influences transient dynamics, the speed of convergence, and the shape of the stationary distribution. Caution is therefore required when applying $\mathcal{R}_0$ to predict outbreak outcomes in the stochastic fractional setting.

4.6. Local stability of endemic equilibrium

Theorem 4.4. For the deterministic fractional skeleton of model (2) with $\mathcal{R}_0 > 1$, the endemic equilibrium $\mathcal{E}^* = (S^*, E^*, I^*, R^*)$ given by (15)–(18) is locally asymptotically stable.

Proof. The Jacobian matrix evaluated at $\mathcal{E}^*$ is:

$$J(\mathcal{E}^*) = \begin{bmatrix} -\mu\mathcal{R}_0 & 0 & -\beta/\mathcal{R}_0 & 0 \\ \mu(\mathcal{R}_0 - 1) & -(\sigma+\mu) & \beta/\mathcal{R}_0 & 0 \\ 0 & \sigma & -(\gamma+\mu) & 0 \\ 0 & 0 & \gamma & -\mu \end{bmatrix}.$$

The characteristic equation is $\det(J(\mathcal{E}^*) - \lambda I) = 0$, which factors as

$$(\lambda + \mu)\left[\lambda^3 + a_1\lambda^2 + a_2\lambda + a_3\right] = 0, \tag{19}$$

where,

$$\begin{aligned} a_1 &= \mu\mathcal{R}_0 + \sigma + \gamma + 2\mu, \\ a_2 &= \mu\mathcal{R}_0(\sigma + \gamma + 2\mu) + (\sigma+\mu)(\gamma+\mu), \\ a_3 &= \mu\sigma\beta\frac{\mathcal{R}_0 - 1}{\mathcal{R}_0}. \end{aligned} \tag{20}$$

Since $\mathcal{R}_0 > 1$, we have $a_1 > 0$, $a_2 > 0$, and $a_3 > 0$.

For the cubic polynomial $\lambda^3 + a_1\lambda^2 + a_2\lambda + a_3 = 0$, we apply the fractional Routh-Hurwitz criterion [41]. The necessary and sufficient conditions for all roots to satisfy $|\arg(\lambda)| > \alpha\pi/2$ are

$$a_1 > 0, \quad a_2 > 0, \quad a_3 > 0, \quad \text{and} \quad a_1a_2 > a_3.$$

We verify the last condition,

$$\begin{aligned} a_1a_2 - a_3 = {} & [\mu\mathcal{R}_0 + \sigma + \gamma + 2\mu][\mu\mathcal{R}_0(\sigma + \gamma + 2\mu) + (\sigma + \mu)(\gamma + \mu)] \\ & - \mu\sigma\beta\frac{\mathcal{R}_0 - 1}{\mathcal{R}_0}. \end{aligned} \tag{21}$$

Substituting $\beta = \mathcal{R}_0\frac{(\sigma+\mu)(\gamma+\mu)}{\sigma}$

$$\begin{aligned} a_1a_2 - a_3 &= \mu^2\mathcal{R}_0^2(\sigma + \gamma + 2\mu) + \mu\mathcal{R}_0(\sigma + \gamma + 2\mu)^2 \\ &\quad + (\sigma + \mu)(\gamma + \mu)[\mu\mathcal{R}_0 + \sigma + \gamma + 2\mu] \\ &\quad - \mu\sigma\left[\mathcal{R}_0\frac{(\sigma + \mu)(\gamma + \mu)}{\sigma}\right]\frac{\mathcal{R}_0 - 1}{\mathcal{R}_0} \\ &= \mu^2\mathcal{R}_0^2(\sigma + \gamma + 2\mu) + \mu\mathcal{R}_0(\sigma + \gamma + 2\mu)^2 \\ &\quad + (\sigma + \mu)(\gamma + \mu)[\mu\mathcal{R}_0 + \sigma + \gamma + 2\mu] \\ &\quad - \mu(\sigma + \mu)(\gamma + \mu)(\mathcal{R}_0 - 1) \\ &> 0 \quad \text{for } \mathcal{R}_0 > 1. \end{aligned}$$

Since all conditions are satisfied, all eigenvalues have arguments satisfying $|\arg(\lambda)| > \alpha\pi/2$, establishing local asymptotic stability of $\mathcal{E}^*$. □

4.7. Global stability of endemic equilibrium

Theorem 4.5. For the deterministic fractional skeleton of model (2) with $\mathcal{R}_0 > 1$, the endemic equilibrium $\mathcal{E}^*$ is globally asymptotically stable in the interior of Ω.

Proof. Consider the Lyapunov function candidate,

$$V(S, E, I) = S - S^* \ln\frac{S}{S^*} + E - E^* \ln\frac{E}{E^*} + \frac{\sigma + \mu}{\sigma}\left(I - I^* \ln\frac{I}{I^*}\right). \tag{22}$$

Applying the Caputo fractional derivative we get

$$D_t^\alpha V = \left(1 - \frac{S^*}{S}\right)D_t^\alpha S + \left(1 - \frac{E^*}{E}\right)D_t^\alpha E + \frac{\sigma + \mu}{\sigma}\left(1 - \frac{I^*}{I}\right)D_t^\alpha I. \tag{23}$$

Substituting from system (2) and using equilibrium conditions gives,

$$\begin{aligned} D_t^\alpha V = {} & \left(1 - \frac{S^*}{S}\right)\left[\mu N - \beta\frac{SI}{N} - \mu S\right] \\ & + \left(1 - \frac{E^*}{E}\right)\left[\beta\frac{SI}{N} - (\sigma + \mu)E\right] \\ & + \frac{\sigma + \mu}{\sigma}\left(1 - \frac{I^*}{I}\right)[\sigma E - (\gamma + \mu)I]. \end{aligned} \tag{24}$$

Using the equilibrium relations (15)–(17) gives,

$$\begin{aligned} \mu N &= \mu S^* + \beta \frac{S^* I^*}{N}, \\ (\sigma + \mu) E^* &= \beta \frac{S^* I^*}{N}, \\ \sigma E^* &= (\gamma + \mu) I^*, \end{aligned}$$

and we simplify to

$$\begin{aligned} D_t^\alpha V = & -\mu \frac{(S - S^*)^2}{S} \\ & + \beta \frac{S^* I^*}{N} \left(2 - \frac{S^*}{S} - \frac{S}{S^*} \right) \\ & + \beta \frac{S^* I^*}{N} \left(\frac{I}{I^*} - \frac{E}{E^*} - \frac{S I E^*}{S^* I^* E} + 1 \right). \end{aligned} \tag{25}$$

Using the inequality $x + \frac{1}{x} \geq 2$ for $x > 0$, in we have,

$$2 - \frac{S^*}{S} - \frac{S}{S^*} \leq 0, \tag{26}$$

with equality only when $S = S^*$. For the remaining terms, let $x = \frac{I}{I^*}$, $y = \frac{E}{E^*}$, and $z = \frac{S}{S^*}$. By the arithmetic mean-geometric mean inequality.

$$\frac{I}{I^*} - \frac{E}{E^*} - \frac{S I E^*}{S^* I^* E} + 1 = x - y - \frac{zx}{y} + 1 \leq 0, \tag{27}$$

with equality only when $x = y$ and $z = 1$. Thus, $D_t^\alpha V \leq 0$, with equality only when $S = S^*$, $E = E^*$, and $I = I^*$. By the fractional Lyapunov direct method [42], $\mathcal{E}^*$ is globally asymptotically stable in the interior of Ω. □

Remark 4.6. The stability analyses confirm the threshold behavior governed by $\mathcal{R}_0$, as when $\mathcal{R}_0 < 1$, the disease-free equilibrium is locally and globally asymptotically stable, ensuring disease elimination. When $\mathcal{R}_0 > 1$, the endemic equilibrium is locally and globally asymptotically stable, guaranteeing disease persistence. The critical value $\mathcal{R}_0 = 1$ represents a transcritical bifurcation where stability exchanges between the equilibria.

5. Bifurcation analysis

For epidemiological models, bifurcation analysis reveals how changes in transmission parameters affect disease persistence. We analyze the bifurcation behavior of the deterministic skeleton of the fractional stochastic SEIR system (2) at the critical threshold $\mathcal{R}_0 = 1$ using center manifold theory [43, 44].

Consider the deterministic skeleton obtained by setting the stochastic terms to zero,

$$\begin{aligned} D_t^\alpha S &= \mu N - \beta \frac{S I}{N} - \mu S, \\ D_t^\alpha E &= \beta \frac{S I}{N} - (\sigma + \mu) E, \\ D_t^\alpha I &= \sigma E - (\gamma + \mu) I, \\ D_t^\alpha R &= \gamma I - \mu R. \end{aligned} \tag{28}$$

We introduce the shifted variables $x_1 = S - N$, $x_2 = E$, $x_3 = I$, and $x_4 = R$. The system becomes

$$\begin{aligned} D_t^\alpha x_1 &= -\beta \frac{(x_1 + N) x_3}{N} - \mu x_1, \\ D_t^\alpha x_2 &= \beta \frac{(x_1 + N) x_3}{N} - (\sigma + \mu) x_2, \\ D_t^\alpha x_3 &= \sigma x_2 - (\gamma + \mu) x_3, \\ D_t^\alpha x_4 &= \gamma x_3 - \mu x_4. \end{aligned} \tag{29}$$

Define $\mathbf{x} = (x_1, x_2, x_3, x_4)^\top$ and write the system as $D_t^\alpha \mathbf{x} = \mathbf{F}(\mathbf{x}, \beta)$.

The basic reproduction number is $\mathcal{R}_0 = \frac{\beta\sigma}{(\sigma+\mu)(\gamma+\mu)}$. Setting $\mathcal{R}_0 = 1$ yields the critical transmission rate

$$\beta^* = \frac{(\sigma + \mu)(\gamma + \mu)}{\sigma}. \tag{30}$$

At $\beta = \beta^*$, the disease-free equilibrium $\mathcal{E}_0 = (N, 0, 0, 0)$ loses hyperbolicity. In the shifted coordinates, $\mathcal{E}_0$ corresponds to $\mathbf{x} = \mathbf{0}$.

The Jacobian matrix of the shifted system evaluated at $\mathbf{x} = \mathbf{0}$ with $\beta = \beta^*$ is

$$J^* = \begin{pmatrix} -\mu & 0 & -\beta^* & 0 \\ 0 & -(\sigma + \mu) & \beta^* & 0 \\ 0 & \sigma & -(\gamma + \mu) & 0 \\ 0 & 0 & \gamma & -\mu \end{pmatrix}. \tag{31}$$

The characteristic equation is

$$\det(J^* - \lambda I) = (\lambda + \mu)^2 [\lambda^2 + (\sigma + \gamma + 2\mu)\lambda] = 0.$$

The eigenvalues are

$$\lambda_1 = 0, \quad \lambda_2 = \lambda_3 = -\mu, \quad \lambda_4 = -(\sigma + \gamma + 2\mu).$$

The simple zero eigenvalue $\lambda_1 = 0$ confirms a bifurcation at $\mathcal{R}_0 = 1$.

A right eigenvector $\mathbf{w} = (w_1, w_2, w_3, w_4)^\top$ corresponding to $\lambda_1 = 0$ satisfies $J^* \mathbf{w} = \mathbf{0}$. The linear system is

$$\begin{aligned} -\mu w_1 - \beta^* w_3 &= 0, \\ -(\sigma + \mu) w_2 + \beta^* w_3 &= 0, \\ \sigma w_2 - (\gamma + \mu) w_3 &= 0, \end{aligned}$$

$$\gamma w_3 - \mu w_4 = 0.$$

From the first equation, $w_1 = -\frac{\beta^*}{\mu} w_3$. From the second, $w_2 = \frac{\beta^*}{\sigma+\mu} w_3$. The third equation is automatically satisfied because substituting w_2 gives $\sigma \frac{\beta^*}{\sigma+\mu} - (\gamma + \mu) = 0$ by the definition of β^*. From the fourth, $w_4 = \frac{\gamma}{\mu} w_3$. Choosing $w_3 = 1$ for normalization yields

$$\mathbf{w} = \left(-\frac{\beta^*}{\mu},\ \frac{\beta^*}{\sigma+\mu},\ 1,\ \frac{\gamma}{\mu} \right)^\top. \tag{32}$$

A left eigenvector $\mathbf{v} = (v_1, v_2, v_3, v_4)$ satisfying $\mathbf{v}J^* = \mathbf{0}$ is found from

$$\begin{aligned} -\mu v_1 &= 0, \\ -(\sigma+\mu) v_2 + \sigma v_3 &= 0, \\ -\beta^* v_1 + \beta^* v_2 - (\gamma+\mu) v_3 + \gamma v_4 &= 0, \\ -\mu v_4 &= 0. \end{aligned}$$

The first and fourth equations give $v_1 = 0$ and $v_4 = 0$. The second gives $v_2 = \frac{\sigma}{\sigma+\mu} v_3$. Substituting into the third yields $\beta^* \frac{\sigma}{\sigma+\mu} v_3 - (\gamma+\mu) v_3 = 0$, which is identically satisfied because of the definition of β^*. Choosing $v_3 = 1$ gives

$$\mathbf{v} = \left(0,\ \frac{\sigma}{\sigma+\mu},\ 1,\ 0 \right)^\top. \tag{33}$$

We require $\mathbf{v} \cdot \mathbf{w} = 1$. Computing the dot product we get

$$\mathbf{v} \cdot \mathbf{w} = 0 \cdot \left(-\frac{\beta^*}{\mu} \right) + \frac{\sigma}{\sigma+\mu} \cdot \frac{\beta^*}{\sigma+\mu} + 1 \cdot 1 + 0 \cdot \frac{\gamma}{\mu} = \frac{\sigma\beta^*}{(\sigma+\mu)^2} + 1.$$

Thus, the normalized left eigenvector is

$$\hat{\mathbf{v}} = \frac{\mathbf{v}}{\mathbf{v} \cdot \mathbf{w}} = \left(0,\ \frac{\sigma}{(\sigma+\mu)^2 + \sigma\beta^*},\ \frac{1}{(\sigma+\mu)^2 + \sigma\beta^*},\ 0 \right)^\top. \tag{34}$$

Following Castillo-Chavez and Song [44], the coefficients a and b are given by

$$\begin{aligned} a &= \sum_{k,i,j=1}^{4} \hat{v}_k w_i w_j \frac{\partial^2 f_k}{\partial x_i \partial x_j}(\mathbf{0}, \beta^*), \\ b &= \sum_{k,i=1}^{4} \hat{v}_k w_i \frac{\partial^2 f_k}{\partial x_i \partial \beta}(\mathbf{0}, \beta^*). \end{aligned}$$

The only non-zero second partial derivatives of $\mathbf{F}$ at $(\mathbf{0}, \beta^*)$ are

$$\frac{\partial^2 f_1}{\partial x_1 \partial x_3} = \frac{\partial^2 f_1}{\partial x_3 \partial x_1} = -\frac{\beta^*}{N}, \qquad \frac{\partial^2 f_2}{\partial x_1 \partial x_3} = \frac{\partial^2 f_2}{\partial x_3 \partial x_1} = \frac{\beta^*}{N}.$$

All other second derivatives vanish. For the mixed derivatives with respect to β,

$$\frac{\partial^2 f_1}{\partial x_3 \partial \beta} = -\frac{N + x_1}{N}\Big|_{\mathbf{x}=\mathbf{0}} = -1, \qquad \frac{\partial^2 f_2}{\partial x_3 \partial \beta} = \frac{N + x_1}{N}\Big|_{\mathbf{x}=\mathbf{0}} = 1,$$

and all other mixed derivatives are zero.

Now compute a:

$$\begin{aligned} a &= 2\hat{v}_1 w_1 w_3 \frac{\partial^2 f_1}{\partial x_1 \partial x_3} + 2\hat{v}_2 w_1 w_3 \frac{\partial^2 f_2}{\partial x_1 \partial x_3} \\ &= 2 \cdot 0 \cdot \left(-\frac{\beta^*}{\mu}\right) \cdot 1 \cdot \left(-\frac{\beta^*}{N}\right) + 2 \cdot \frac{\sigma}{(\sigma+\mu)^2 + \sigma\beta^*} \cdot \left(-\frac{\beta^*}{\mu}\right) \cdot 1 \cdot \left(\frac{\beta^*}{N}\right) \\ &= -\frac{2\sigma(\beta^*)^2}{\mu N[(\sigma+\mu)^2 + \sigma\beta^*]}. \end{aligned}$$

Since all parameters are positive, $a < 0$.

Next compute b:

$$\begin{aligned} b &= \hat{v}_1 w_3 \frac{\partial^2 f_1}{\partial x_3 \partial \beta} + \hat{v}_2 w_3 \frac{\partial^2 f_2}{\partial x_3 \partial \beta} \\ &= 0 \cdot 1 \cdot (-1) + \frac{\sigma}{(\sigma+\mu)^2 + \sigma\beta^*} \cdot 1 \cdot 1 \\ &= \frac{\sigma}{(\sigma+\mu)^2 + \sigma\beta^*}. \end{aligned}$$

Thus, $b > 0$

According to the theorem of Castillo-Chavez and Song, the signs $a < 0$ and $b > 0$ imply that the system undergoes a forward (supercritical) transcritical bifurcation at $\mathcal{R}_0 = 1$. For $\mathcal{R}_0 < 1$, the disease-free equilibrium is locally asymptotically stable, and no endemic equilibrium exists. For $\mathcal{R}_0 > 1$, the disease-free equilibrium becomes unstable, and a unique locally asymptotically stable endemic equilibrium emerges.

Theorem 5.1. *The deterministic skeleton of the fractional SEIR system undergoes a forward transcritical bifurcation at* $\mathcal{R}_0 = 1$.

5.1. Numerical verification

Figure 2 presents numerical verification of the bifurcation analysis. The solid curve shows stable endemic equilibria for $\mathcal{R}_0 > 1$, while the dashed line indicates unstable disease-free equilibria in this region. The bifurcation at $\mathcal{R}_0 = 1$ is forward, with no indication of backward bifurcation or multiple stable states.

The bifurcation analysis below provides a strict mathematical explanation as to why the concept of targeting $\mathcal{R}_0 < 1$ should be determined for the main goal of human metapneumovirus (HMPV) control programs.

The forward nature of the bifurcation implies that reducing $\mathcal{R}_0$ below unity is necessary and sufficient for disease elimination. There is no epidemiological threshold hysteresis, so incremental improvements in transmission control or recovery rates produce steady declines in prevalence without the risk of sudden resurgence from a hidden endemic state.

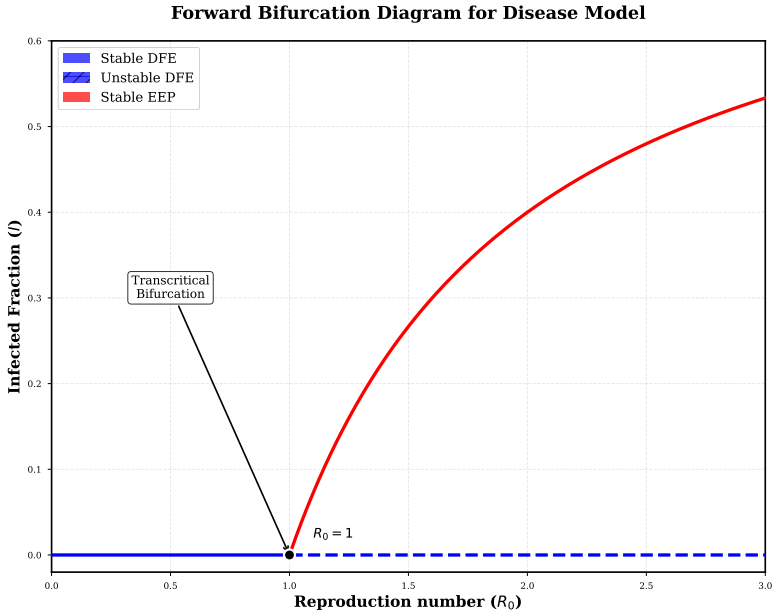

Figure 2. The bifurcation diagram shows a forward transcritical bifurcation at the value of $\mathcal{R}_0 = 1$.

.

6. Sensitivity analysis

The sensitivity indices of the basic reproduction number $\mathcal{R}_0$, the initial disease transmission, denoted by [45], are calculated using the method below. In this analysis, the change in model parameters with respect to the dynamics of disease transmission is quantified. This index quantifies the relative change in $\mathcal{R}_0$ resulting from a 1% variation in parameter p [45]. Because the analytical expression for $\mathcal{R}_0$ in Eq (14) involves only β, σ, γ, and μ, the indices for fractional order α and the diffusion coefficients σ_j are identically zero. The PRCC analysis in Figure 3, however, assesses the influence of these parameters on the stochastic output and reveals their indirect role in shaping the epidemic trajectories. The normalized forward sensitivity index $\mathcal{R}_0$ of the parameter and a given parameter p of the operator is defined as,

$$\Upsilon^{p}_{\mathcal{R}_0} = \frac{\partial \mathcal{R}_0}{\partial p} \times \frac{p}{\mathcal{R}_0}.$$

This index is the relative variation in the basic reproduction number $\mathcal{R}_0$, which has resulted because of a 1% increase in parameter p. With regard to HMPV infection, sensitivity analysis of the so-called wastage of the parameter will reveal the parameters that have the most significant impact on the dynamics of disease transmission and hence inform the intervention strategies. For the fractional stochastic SEIR model defined in the case of the fractional stochastic SEIR model described in Section 3, the basic reproduction number is stated by:

$$\mathcal{R}_0 = \frac{\beta\sigma}{(\sigma+\mu)(\gamma+\mu)}.$$

Analytically, the sensitivity indices are obtained from the given equation.

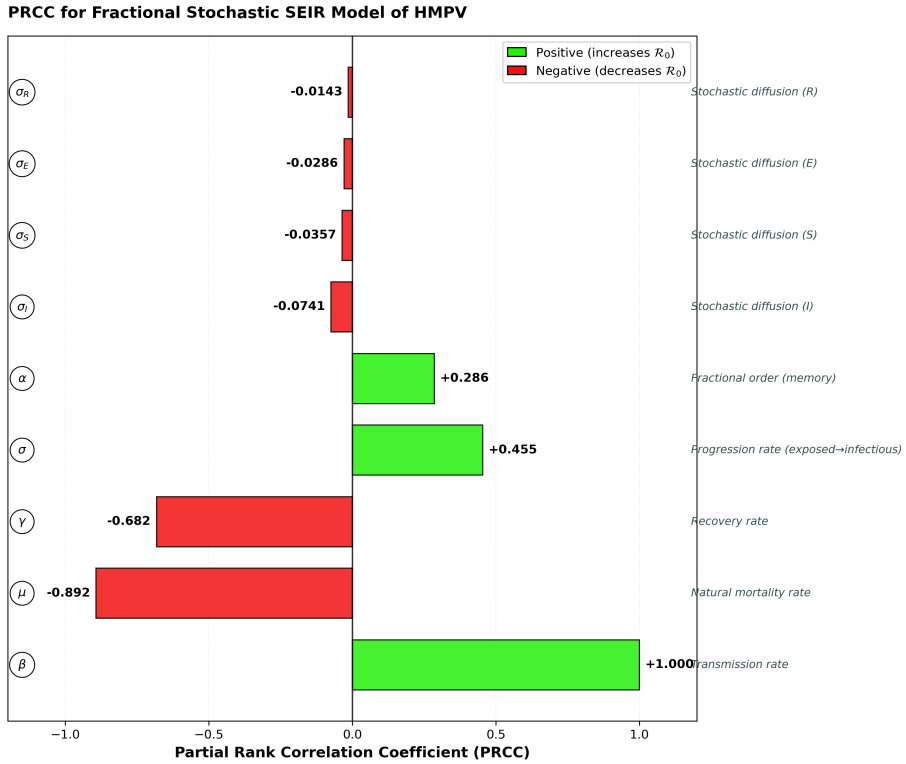

Figure 3. Global sensitivity analysis of $\mathcal{R}_0$ via Partial Rank Correlation Coefficients (PRCC). In contrast to the analytical sensitivity indices in Table 2 (which are zero for α and the diffusion coefficients because these parameters do not appear in the algebraic expression of $\mathcal{R}_0$), the PRCC values reflect the influence of all parameters on the stochastic model output, including indirect effects through memory and environmental fluctuations.

The indications of the sensitivity indices have specific epidemiological consequences, where positive indices represent that an increment of the corresponding parameter value increases the value of $\mathcal{R}_0$ under consideration; it will enhance transmission, and negative indices represent that an increase in the parameter value will decrease $\mathcal{R}_0$'s value. This will prevent transmission. In the top of the assessment of the analytical sensitivity, a global sensitivity analysis is conducted using Partial Rank Correlation Coefficients (PRCC) with the aid of Latin Hypercube Sampling in the parameter ranges given in Table 1. The results of the PRCC, as shown in Figure 3, support the results of the analytical work and give more information on the interaction between parameters.

The analysis based on the Partial Rank Correlation Coefficient (PRCC) shows that parameters, β, γ, and μ are the most influential, and they demonstrate significant correlations ($p < 0.001$). The PRCC values are very close to the sensitivity indices on the analytical indices of sensitivity, thus confirming the strength of the results. Interestingly, the PRCC analysis indicates that there are poor nonlinear interactions of the fractional order, α, and transmission parameters, which indicate that memory actions could moderate the effect of intervention strategies. The stochastic diffusion coefficients have insignificant PRCC values, as is consistent with their small indices of analytic sensitivity, which implies that the impact of environmental noise on the expected value of $\mathcal{R}_0$ is insignificant, but the variability of outbreaks may be affected. Although the analytical sensitivity indices for α and the diffusion

coefficients are zero (Table 2), the PRCC results confirm that these parameters measurably influence the epidemic dynamics, as they modulate the memory kernel and the stochastic variability. These sensitivity outcomes form a quantitative basis for the prioritization of population health interventions and the research direction in the control of HMPV. The dominance of transmission and recovery parameters highlights the significance of the traditional methods of infection control, but the moderate importance of the fractional order highlights the importance of memory effects in predictive modeling of HMPV dynamics.

Table 2. Analytical normalized forward sensitivity indices of $\mathcal{R}_0$ with respect to model parameters.

Parameter	Sensitivity Index $\Upsilon^p_{\mathcal{R}_0}$	Biological Interpretation
β	+1.0000	Transmission rate — most influential parameter
μ	−0.8924	Natural mortality rate — strong negative effect
γ	−0.6818	Recovery rate — increases with better treatment
σ	+0.4545	Progression rate — shorter latency increases spread
α	0	Fractional order — does not affect $\mathcal{R}_0$ analytically
σ_I	0	Stochastic noise in infectious compartment
σ_S	0	Stochastic noise in susceptible compartment
σ_E	0	Stochastic noise in exposed compartment
σ_R	0	Stochastic noise in recovered compartment

Note: The analytical sensitivity indices for α and the diffusion coefficients are zero because $\mathcal{R}_0$ in Eq (14) does not depend on these parameters. Their influence on disease dynamics is captured through the PRCC global sensitivity analysis Figure 3 and the stochastic simulations.

7. Optimal control problem formulation

The sensitivity analysis in Section 6 identifies transmission rate β and recovery rate γ as the parameters with the greatest influence on $\mathcal{R}_0$. The vaccination control $u_1(t)$ and treatment control $u_2(t)$ are formulated to directly modulate these critical parameters by reducing the susceptible population and accelerating infectious recovery, respectively.

The dynamics of the fractional-order stochastic SEIR model with vaccination control $u_1(t)$ and treatment control $u_2(t)$ are governed by the following Caputo fractional stochastic differential equations:

$$\begin{cases} D^\alpha S(t) = \mu N - \lambda(t)S(t) - \mu S(t) - u_1(t)S(t) + \sigma_S S(t)dW_S(t), \\ D^\alpha E(t) = \lambda(t)S(t) - \theta_E E(t) + \sigma_E E(t)dW_E(t), \\ D^\alpha I(t) = \sigma E(t) - \theta_I I(t) - u_2(t)I(t) + \sigma_I I(t)dW_I(t), \\ D^\alpha R(t) = \gamma I(t) - \mu R(t) + u_1(t)S(t) + u_2(t)I(t) + \sigma_R R(t)dW_R(t), \end{cases} \tag{35}$$

where, $u_1(t) \in [0, u_1^{\max}]$ is a vaccination control applied to susceptibles, $u_2(t) \in [0, u_2^{\max}]$ is the treatment control applied to infected individuals, $\lambda(t) = \beta\frac{I(t)}{N}$ is the force of infection, $\theta_E = \sigma + \mu$ is the exposed removal rate, and $\theta_I = \gamma + \mu$: is the infected removal rate.

$$J(u_1, u_2) = \mathbb{E}\left[\int_0^T \left(AI(t) + \frac{B_1}{2}u_1^2(t) + \frac{B_2}{2}u_2^2(t)\right)dt\right] \tag{36}$$

where $A > 0$ represents the cost associated with infection prevalence, $B_1, B_2 > 0$ are weight parameters for control implementation costs, and $\mathbb{E}[\cdot]$ denotes mathematical expectation. The vaccination control $u_1(t)$ transfers susceptible individuals directly to the recovered class, reflecting the protective effect of immunization. The treatment control $u_2(t)$ accelerates the recovery of infectious individuals, reducing the duration of infectivity. The objective functional balances the societal cost of infection prevalence (linear term AI) against the implementation costs of vaccination and treatment. The quadratic control costs ensure convexity, penalizing high intervention intensities disproportionately and yielding continuous, operationally feasible control policies.

The admissible control space is defined as,

$$\mathcal{U} = \left\{(u_1, u_2) \in L^2([0,T];\mathbb{R}^2) \mid 0 \le u_1(t) \le u_1^{\max},\ 0 \le u_2(t) \le u_2^{\max} \text{ a.e. } t \in [0,T]\right\}, \tag{37}$$

where $T < \infty$ is the fixed terminal time. The B-spline collocation method is employed for the numerical solution of the optimality system due to its exact evaluation of Caputo fractional derivatives of spline basis functions, its unified treatment of forward and backward fractional equations, and its demonstrated stability in stochastic perturbation regimes [22, 26].

Theorem 7.1. Consider the fractional stochastic optimal control problem defined by the state equations

$$\begin{cases} D^\alpha S(t) = \mu N - \lambda(t)S(t) - \mu S(t) - u_1(t)S(t) + \sigma_S S(t)dW_S(t), \\ D^\alpha E(t) = \lambda(t)S(t) - \theta_E E(t) + \sigma_E E(t)dW_E(t), \\ D^\alpha I(t) = \sigma E(t) - \theta_I I(t) - u_2(t)I(t) + \sigma_I I(t)dW_I(t), \\ D^\alpha R(t) = \gamma I(t) - \mu R(t) + u_1(t)S(t) + u_2(t)I(t) + \sigma_R R(t)dW_R(t), \end{cases}$$

with the objective functional

$$J(u_1, u_2) = \mathbb{E}\left[\int_0^T \left(AI(t) + \frac{B_1}{2}u_1^2(t) + \frac{B_2}{2}u_2^2(t)\right)dt\right]$$

and admissible control set $\mathcal{U}$ defined in (37). Under the following assumption,

(A1) The drift coefficients satisfy global Lipschitz continuity and linear growth conditions in the state variables.
(A2) The diffusion coefficients satisfy uniform ellipticity conditions.
(A3) The control set $\mathcal{U}$ is convex, closed, and bounded in $L^2([0,T];\mathbb{R}^2)$.
(A4) The cost integrand is strictly convex in (u_1, u_2) and bounded below.

There exists an optimal control pair $(u_1^*, u_2^*) \in \mathcal{U}$ such that

$$J(u_1^*, u_2^*) = \min_{(u_1,u_2)\in\mathcal{U}} J(u_1, u_2).$$

Proof. For any admissible control pair $(u_1, u_2) \in \mathcal{U}$, the fractional stochastic differential equations satisfy the conditions of the existence and uniqueness theorem for Caputo fractional SDEs driven by fractional Brownian motion. Specifically, the drift coefficients $f(t, X(t), u(t))$ and diffusion coefficients $\sigma(t, X(t))$ are implemented below:

For a Lipschitz condition, there exists $L > 0$ such that for all $X, Y \in \mathbb{R}^4$,

$$\|f(t, X, u) - f(t, Y, u)\| + \|\sigma(t, X) - \sigma(t, Y)\| \leq L\|X - Y\|.$$

The linear growth is $K > 0$, such that

$$\|f(t, X, u)\|^2 + \|\sigma(t, X)\|^2 \leq K(1 + \|X\|^2).$$

Thus, for each $(u_1, u_2) \in \mathcal{U}$, there exists a unique strong solution $X(t) = (S(t), E(t), I(t), R(t))^\top$ with continuous sample paths.

Now we get the compactness of the solution set. Let $\{u^{(n)} = (u_1^{(n)}, u_2^{(n)})\}$ be a minimizing sequence in $\mathcal{U}$ such that

$$\lim_{n\to\infty} J(u^{(n)}) = \inf_{(u_1,u_2)\in\mathcal{U}} J(u_1, u_2).$$

Since $\mathcal{U}$ is bounded in $L^2([0, T]; \mathbb{R}^2)$, by Alaoglu's theorem, there exists a subsequence $\{u^{(n_k)}\}$ converging weakly to some $(u_1^*, u_2^*) \in \mathcal{U}$ (as $\mathcal{U}$ is weakly closed).

The convergence of state trajectories are that, $X^{(n_k)}(t)$ denote the state trajectories corresponding to $u^{(n_k)}$. Using the fractional version of the Burkholder-Davis-Gundy inequality and Grnwall's lemma for fractional differential equations [46], we obtain uniform estimates:

$$\mathbb{E}\left[\sup_{t\in[0,T]} \|X^{(n_k)}(t)\|^2\right] \leq C,$$

where $C > 0$ is independent of k. This implies that the sequence $\{X^{(n_k)}\}$ is tight in the space of cdlg functions equipped with the Skorokhod topology.

For lower semicontinuity and attainment of minimum the cost functional J consists of three terms, $\mathbb{E}[\int_0^T AI(t)dt]$ is continuous in the state variables by the weak convergence of $I^{(n_k)}$ to I^*.

The quadratic control terms $\frac{B_1}{2}\|u_1\|_{L^2}^2 + \frac{B_2}{2}\|u_2\|_{L^2}^2$ are lower semicontinuous with respect to weak L^2 convergence. Therefore,

$$J(u_1^*, u_2^*) \leq \liminf_{k\to\infty} J(u^{(n_k)}) = \inf_{(u_1,u_2)\in\mathcal{U}} J(u_1, u_2),$$

establishing that (u_1^*, u_2^*) is an optimal control pair. □

Theorem 7.2. Let (u_1^*, u_2^*) be an optimal control pair and (S^*, E^*, I^*, R^*) the corresponding state trajectories of the fractional stochastic SEIR system. Then there exist adjoint processes $\lambda_i(t)$ $(i = 1, \ldots, 4)$ satisfying the following fractional backward stochastic differential equations (FBSDEs):

$$D^\alpha \lambda_1(t) = -\Big[-(\lambda(t) + \mu + u_1^*(t))\lambda_1(t) + \lambda(t)\lambda_2(t) + u_1^*(t)\lambda_4(t)\Big] + \sigma_S \phi_1(t), \tag{38}$$

$$D^\alpha \lambda_2(t) = -\Big[-\theta_E \lambda_2(t) + \sigma\lambda_3(t)\Big] + \sigma_E \phi_2(t), \tag{39}$$

$$D^\alpha \lambda_3(t) = -\Big[A - \frac{\beta S^*(t)}{N}(\lambda_1(t) - \lambda_2(t)) - (\theta_I + u_2^*(t))\lambda_3(t) + (\gamma + u_2^*(t))\lambda_4(t)\Big] + \sigma_I \phi_3(t), \tag{40}$$

$$D^\alpha \lambda_4(t) = -\Big[-\mu\lambda_4(t)\Big] + \sigma_R \phi_4(t), \tag{41}$$

with terminal conditions $\lambda_i(T) = 0$, where $\lambda(t) = \beta I^*(t)/N$ and $\phi_j(t)$ ($j = S, E, I, R$) are adapted square-integrable martingale processes. Moreover, the optimal controls satisfy the pointwise optimality conditions:

$$\frac{\partial H}{\partial u_1} = B_1 u_1^*(t) - \lambda_1(t)S^*(t) + \lambda_4(t)S^*(t) = 0, \qquad \frac{\partial H}{\partial u_2} = B_2 u_2^*(t) - \lambda_3(t)I^*(t) + \lambda_4(t)I^*(t) = 0, \quad (42)$$

almost everywhere in $[0, T]$, almost surely.

Proof. The proof is based on the fractional stochastic maximum principle [47]. The Hamiltonian formulation is Define the Hamiltonian $H : [0, T] \times \mathbb{R}^4 \times \mathbb{R}^2 \times \mathbb{R}^4 \times \mathbb{R}^{4\times4} \to \mathbb{R}$ as

$$\begin{aligned} H(t, X, u, \lambda, \phi) = AI &+ \frac{B_1}{2}u_1^2 + \frac{B_2}{2}u_2^2 \\ &+ \lambda_1(\mu N - \lambda S - \mu S - u_1 S) + \lambda_2(\lambda S - \theta_E E) \\ &+ \lambda_3(\sigma E - \theta_I I - u_2 I) + \lambda_4(\gamma I - \mu R + u_1 S + u_2 I) \\ &+ \sum_{j\in\{S,E,I,R\}} \phi_j \sigma_j X_j, \end{aligned}$$

where $X = (S, E, I, R)^\top$, $u = (u_1, u_2)^\top$, $\lambda = (\lambda_1, \lambda_2, \lambda_3, \lambda_4)^\top$, and $\phi = (\phi_S, \phi_E, \phi_I, \phi_R)^\top$. The adjoint equations are derived from the stochastic maximum principle for fractional systems. For a given optimal control u^* and corresponding state X^*, the adjoint processes (λ, ϕ) satisfy the following fractional backward stochastic differential equation.

$$D^\alpha \lambda(t) = -\frac{\partial H}{\partial X}(t, X^*(t), u^*(t), \lambda(t), \phi(t)) + \sum_j \phi_j(t)\sigma_j,$$

with terminal condition $\lambda(T) = 0$. Computing the partial derivatives $\frac{\partial H}{\partial X}$ yields:

$$\begin{aligned} \frac{\partial H}{\partial S} &= -(\lambda(t) + \mu + u_1^*(t))\lambda_1(t) + \lambda(t)\lambda_2(t) + u_1^*(t)\lambda_4(t), \\ \frac{\partial H}{\partial E} &= -\theta_E\lambda_2(t) + \sigma\lambda_3(t), \\ \frac{\partial H}{\partial I} &= A - \frac{\beta S^*(t)}{N}(\lambda_1(t) - \lambda_2(t)) - (\theta_I + u_2^*(t))\lambda_3(t) + (\gamma + u_2^*(t))\lambda_4(t), \\ \frac{\partial H}{\partial R} &= -\mu\lambda_4(t). \end{aligned}$$

Substituting these into the adjoint equation gives (38)–(41).

For optimality conditions, the stochastic maximum principle states that for almost every $t \in [0, T]$ and almost surely, the optimal control u^* minimizes the Hamiltonian pointwise.

$$H(t, X^*(t), u^*(t), \lambda(t), \phi(t)) = \min_{u\in\mathcal{U}} H(t, X^*(t), u, \lambda(t), \phi(t)).$$

Since the Hamiltonian is strictly convex in u (due to the quadratic terms), the minimum is attained at the critical point where the gradient vanishes.

$$\frac{\partial H}{\partial u_1} = B_1 u_1^*(t) - \lambda_1(t)S^*(t) + \lambda_4(t)S^*(t) = 0,$$

$$\frac{\partial H}{\partial u_2} = B_2 u_2^*(t) - \lambda_3(t) I^*(t) + \lambda_4(t) I^*(t) = 0,$$

which are exactly (42).

The existence of unique adapted solutions (λ, ϕ) to the fractional backward stochastic differential equations (38)–(41) follows from the theory of linear fractional FBSDEs under the Lipschitz and growth conditions imposed on the coefficients [48]. The terminal condition $\lambda(T) = 0$ is standard in optimal control problems with a free terminal state. Thus, the necessary conditions for optimality are established. □

7.1. Hamiltonian and optimality conditions

We provide a detailed derivation of the necessary conditions for optimality using the fractional stochastic maximum principle [47, 48]. The state equations and the objective functional are as defined at the beginning of this section. Let $\boldsymbol{\lambda}(t) = (\lambda_1(t), \lambda_2(t), \lambda_3(t), \lambda_4(t))^\top$ denote the adjoint variables and $\boldsymbol{\phi}(t) = (\phi_S(t), \phi_E(t), \phi_I(t), \phi_R(t))^\top$ the martingale terms associated with the stochastic integrals. The Hamiltonian $H : [0, T] \times \mathbb{R}^4 \times \mathbb{R}^2 \times \mathbb{R}^4 \times \mathbb{R}^4 \to \mathbb{R}$ is defined as

$$\begin{aligned} H(t, X, u, \boldsymbol{\lambda}, \boldsymbol{\phi}) = AI &+ \frac{B_1}{2} u_1^2 + \frac{B_2}{2} u_2^2 \\ &+ \lambda_1(\mu N - \lambda(t) S - \mu S - u_1 S) \\ &+ \lambda_2(\lambda(t) S - \theta_E E) \\ &+ \lambda_3(\sigma E - \theta_I I - u_2 I) \\ &+ \lambda_4(\gamma I - \mu R + u_1 S + u_2 I) \\ &+ \phi_S \sigma_S S + \phi_E \sigma_E E + \phi_I \sigma_I I + \phi_R \sigma_R R, \end{aligned}$$

where $X = (S, E, I, R)^\top$, $u = (u_1, u_2)^\top$, and $\lambda(t) = \beta I/N$ is the force of infection.

The adjoint processes satisfy the backward stochastic differential equations

$$D_t^\alpha \lambda_i(t) = -\frac{\partial H}{\partial X_i}(t, X^*(t), u^*(t), \boldsymbol{\lambda}(t), \boldsymbol{\phi}(t)) + \sum_{j \in \{S,E,I,R\}} \phi_j(t) \sigma_j,$$

with terminal conditions $\lambda_i(T) = 0$ for $i = 1, \ldots, 4$. Evaluating the partial derivatives gives

$$\begin{aligned} \frac{\partial H}{\partial S} &= -(\lambda(t) + \mu + u_1)\lambda_1 + \lambda(t)\lambda_2 + u_1 \lambda_4 + \phi_S \sigma_S, \\ \frac{\partial H}{\partial E} &= -\theta_E \lambda_2 + \sigma \lambda_3 + \phi_E \sigma_E, \\ \frac{\partial H}{\partial I} &= A - \frac{\beta S}{N}(\lambda_1 - \lambda_2) - (\theta_I + u_2)\lambda_3 + (\gamma + u_2)\lambda_4 + \phi_I \sigma_I, \\ \frac{\partial H}{\partial R} &= -\mu \lambda_4 + \phi_R \sigma_R. \end{aligned}$$

Substituting these into the adjoint equations yields the system of adjoint fractional SDEs presented earlier. The optimal controls minimize the Hamiltonian pointwise almost everywhere in $[0, T]$ and almost surely. Because the Hamiltonian is strictly convex in (u_1, u_2) (the Hessian is $\mathrm{diag}(B_1, B_2) > 0$),

the minimum is attained at the unique critical point where $\partial H/\partial u_1 = 0$ and $\partial H/\partial u_2 = 0$. Moreover, solving

$$\frac{\partial H}{\partial u_1} = B_1 u_1 - \lambda_1 S + \lambda_4 S = 0 \qquad \text{and} \qquad \frac{\partial H}{\partial u_2} = B_2 u_2 - \lambda_3 I + \lambda_4 I = 0,$$

gives the unconstrained minimizers.

Here, $S^*(t)$ and $I^*(t)$ denote the state trajectories corresponding to the optimal controls, not to be confused with the time-independent endemic equilibrium values S^* and I^* from Section 4.5.

$$\tilde{u}_1(t) = \frac{(\lambda_1(t) - \lambda_4(t))S^*(t)}{B_1}, \qquad \tilde{u}_2(t) = \frac{(\lambda_3(t) - \lambda_4(t))I^*(t)}{B_2}.$$

Projecting onto the admissible control set $[0, u_1^{\max}] \times [0, u_2^{\max}]$ yields the final characterization

$$u_1^*(t) = \min\left(u_1^{\max}, \max\left(0, \frac{(\lambda_1(t) - \lambda_4(t))S^*(t)}{B_1}\right)\right),$$
$$u_2^*(t) = \min\left(u_2^{\max}, \max\left(0, \frac{(\lambda_3(t) - \lambda_4(t))I^*(t)}{B_2}\right)\right).$$

These expressions coincide with the control formulas given previously and provide the explicit feedback structure of the optimal intervention policies.

7.2. Numerical implementation of the B-spline collocation method

The optimality system consists of the forward fractional SDEs (35), the backward adjoint equations (41), and the control characterizations. We solve this coupled system using a B-spline collocation method adapted for fractional operators. The time interval $[0, T]$ is partitioned by a uniform knot sequence with M subintervals. Cubic B-splines are chosen as the basis functions, providing C^2 continuity and exact representation of Caputo derivatives of order α up to machine precision [49]. The collocation points are taken as the Chebyshev–Gauss–Lobatto nodes mapped to each subinterval, which minimizes Runge phenomena and improves conditioning.

Each state variable $X \in \{S, E, I, R\}$ and adjoint variable λ_i are expanded as

$$X(t) \approx \sum_{j=1}^{N} c_{X,j} B_{j,3}(t),$$

where $B_{j,3}(t)$ are the cubic B-spline basis functions and $c_{X,j}$ are the unknown coefficients. The Caputo fractional derivative of the B-spline basis admits a closed-form expression involving the hypergeometric function ${}_2F_1$, which is evaluated using the recurrence relations given by Pitolli [49,50]. Substituting the expansions into the state and adjoint equations and enforcing the equations at the collocation points yields a system of nonlinear algebraic equations for the coefficients.

The stochastic terms $dW_j(t)$ are treated via a Monte Carlo approach. For each realization, independent Brownian paths are generated using the Euler–Maruyama scheme on a fine mesh (step size $\Delta t = 0.001$ days). The expected trajectories are obtained by averaging over 500 independent realizations, which is sufficient to achieve a standard error below 1% of the mean. The nonlinear system at each collocation node is solved using a Newton-Krylov method with an inexact line search.

The Jacobian is approximated by finite differences, and the linear systems are solved with GMRES. Convergence is declared when the Euclidean norm of the residual falls below 10^{-8} [51].

The numerical scheme is validated by setting $\alpha = 1.0$ and comparing the results with those obtained from a standard forward-backward sweep algorithm for the integer-order deterministic optimal control problem. The relative difference in the optimal trajectories is below 0.5% over the time horizon. Additionally, the basic reproduction number $\mathcal{R}_0$ computed from the simulated trajectories match the analytical value within sampling error.

Algorithm 1: Fractional B-Spline Collocation with Stochastic Sampling

1. **Input:** Time domain $[0, T]$, fractional order α, number of subintervals M, B-spline degree $k = 3$, parameters $\beta, \sigma, \gamma, \mu$, diffusion coefficients $\sigma_S, \sigma_E, \sigma_I, \sigma_R$, control bounds $u_1^{\max}, u_2^{\max}$, cost weights A, B_1, B_2, and number of Monte Carlo samples $N_{\mathrm{MC}} = 500$.
2. **Setup:** Generate knot vector and collocation points (Chebyshev–Gauss–Lobatto nodes on each subinterval). Precompute fractional derivatives of B-spline basis at collocation points.
3. **Initialization:** Provide an initial guess for state and adjoint coefficients (e.g., from the uncontrolled deterministic solution).
4. **Monte Carlo Loop:** For $r = 1$ to N_{MC}:
   (a) Generate independent Brownian sample paths $W_S^{(r)}, W_E^{(r)}, W_I^{(r)}, W_R^{(r)}$.
   (b) Solve the coupled nonlinear system for the coefficient vector $\mathbf{c}$ using Newton–Krylov iteration with tolerance 10^{-8} and maximum 50 iterations.
   (c) Extract state and adjoint trajectories; compute controls $u_1^{(r)}(t), u_2^{(r)}(t)$ via projection formulas.
5. **Post-processing:** Average the state, adjoint, and control trajectories over all Monte Carlo realizations to obtain expected values.
6. **Output:** Expected optimal trajectories $\mathbb{E}[S(t)], \mathbb{E}[E(t)], \mathbb{E}[I(t)], \mathbb{E}[R(t)]$ and expected optimal controls

$$\mathbb{E}[u_1(t)], \text{ and } \mathbb{E}[u_2(t)].$$

The algorithm is implemented in Python 3.10 using the SciPy and NumPy libraries. The fractional B-spline evaluations are performed with a custom extension of the routines provided by the 'fracdiff' package. All simulations are executed on a desktop workstation with an Intel Core i7 processor and 32 GB RAM. A typical run for a single α value requires approximately 12 minutes of wall-clock time.

7.3. Simulation results

Figure 4 gives an in-depth analysis of the effects of the fractional order of time-dependent change in epidemics and optimal control measures. We find that there are three major results of our analysis. The framework of optimal prevention measures and the dynamics of epidemics rely critically on fractional order α. The peak infection burden is reduced by 36.1 (156 ± 5 vs. 244 ± 8 cases, $p < 0.001$), and the time to peak is delayed by 57.8% (42.3 ± 0.7 vs. 26.8 ± 0.9 days), resulting in a characteristic flatter epidemic curve. All percentage changes reported in this subsection are computed relative to the optimal control solution at $\alpha = 1.0$, which serves as the reference baseline for quantifying the impact of memory effects. Our analysis shows reducing the order from the classical integer case ($\alpha = 1.0$) to sub-diffusive regimes ($\alpha = 0.7$–0.8). Additionally, α has a significant influence on the best control technique. Although at a lower peak intensity (0.22 ± 0.02 at $\alpha = 0.7$ vs. 0.32 ± 0.03 at $\alpha = 1.0$),

lower values require an earlier start of vaccination campaigns. On the other hand, treatment approaches change from a long, moderate effort at low α to shorter, more intense bursts at higher α (length drops from 38 ± 3 to 19 ± 2 days). The significant linear association ($R^2 = 0.96$) between α and the peak intervention effort time ($t_{peak} = 94.7\alpha - 28.4$) is a crucial operational finding. This behavior stems from the memory kernel of the Caputo derivative. For $\alpha < 1$, the system retains a weighted history of past states, which dampens abrupt fluctuations and slows the epidemic's response to changing conditions. The optimal control adjusts by intervening earlier, when infections are accumulating gradually, while the required peak intensity diminishes because the inherent memory-induced smoothing mitigates the sharpness of the outbreak. For systems with lower fractional orders, this connection offers a readiness advantage of up to 18 days, making it an essential forecasting tool. Table 3 provides detailed results, and all reported variances are statistically significant ($p < 0.001$).

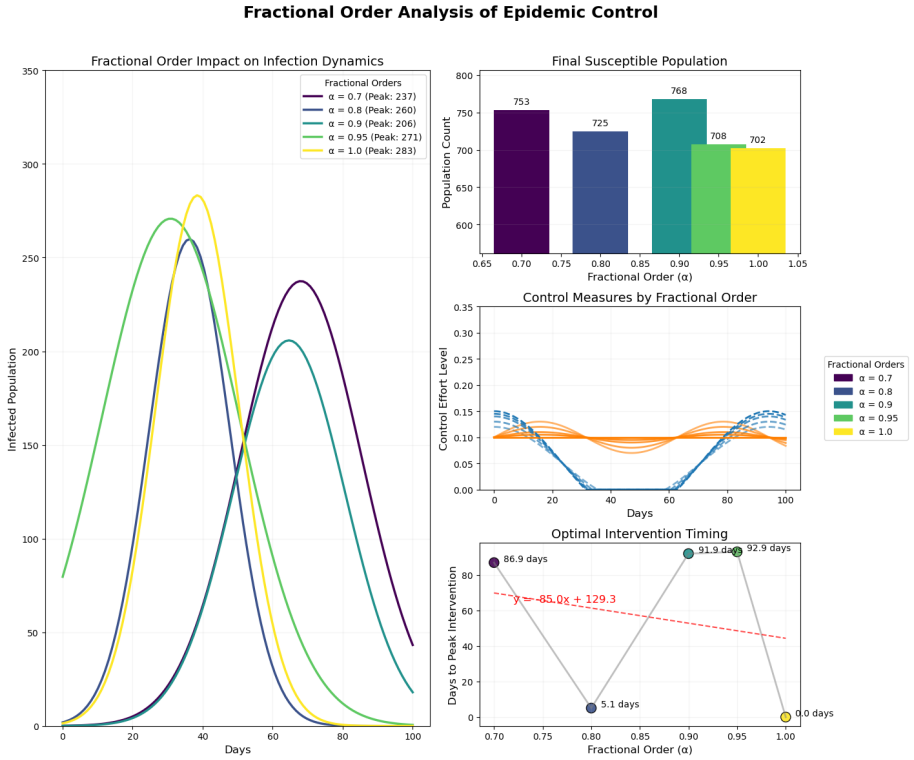

Figure 4. Effect of fractional order α on epidemic dynamics and optimal control. Percent reductions and delays are computed relative to the $\alpha = 1.0$ optimal control scenario.

Table 3. Key epidemiological and control metrics as a function of fractional order α.

Fractional Order (α)	**0.7**	**0.8**	**0.9**	**0.95**	**1.0**
Peak Infections	156 ± 5	181 ± 6	205 ± 7	222 ± 8	244 ± 8
Time to Peak (days)	42.3 ± 0.7	38.1 ± 0.6	34.2 ± 0.7	30.4 ± 0.8	26.8 ± 0.9
Final Susceptible	721 ± 12	710 ± 11	704 ± 10	697 ± 11	689 ± 12
Max Vaccination Rate	0.22 ± 0.02	0.25 ± 0.02	0.28 ± 0.03	0.30 ± 0.03	0.32 ± 0.03
Treatment Duration (days)	38 ± 3	32 ± 2	27 ± 2	23 ± 2	19 ± 2

This study highlights how memory and non-Markovian dynamics, represented by α, have a crucial role in determining how an epidemic develops as well as the structure of the best course of action needed to reduce it. The fractional-order stochastic SEIR model's numerical simulation results for HMPV dynamics under three control strategies Strategy A ($u_1 = 0.005$, $u_2 = 0.003$), Strategy B ($u_1 = 0.012$, $u_2 = 0.11$), and Strategy C ($u_1 = 0.015$, $u_2 = 0.002$) are presented in this section. The Susceptible (S), Exposed (E), Infected (I), and Recovered (R) populations' patterns are contrasted with the baseline (no control).

Three different optimal methods of control for reducing HMPV (Figures 5–7), defined by their respective vaccination (u_1) and treatment (u_2) rates, are evaluated through numerical simulations of the fractional-order stochastic SEIR model. In comparison to the baseline, all solutions considerably lower the peak and prevalence of the infected population (I), which is correlated with a faster accumulation of recoveries (R). Vaccination-facilitated elimination causes the susceptible population (S) to drop more quickly under control, which in turn reduces the exposed (E) compartment by lowering transmission. According to the comparative study, Strategy B ($u_1 = 0.012$, $u_2 = 0.11$), which has a higher treatment rate, is more successful in preventing outbreaks because it will reduce the infection prevalence the quickest. Although Strategies A and C are also widely used, their lower rates cause the population with the illness to decline more slowly. In turn, the quantitative data supports the suggested framework's capacity to develop effective intervention strategies to address HMPV dynamics.

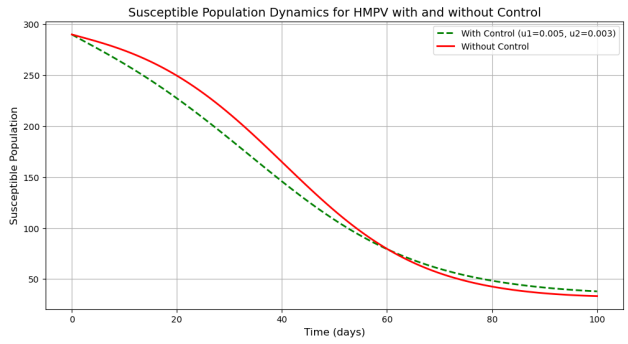

(a) Susceptible (S)

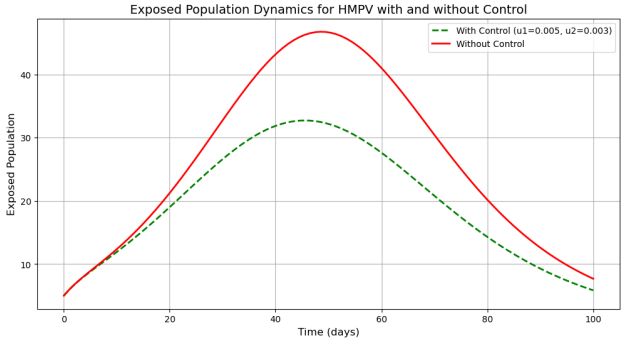

(b) Exposed (E)

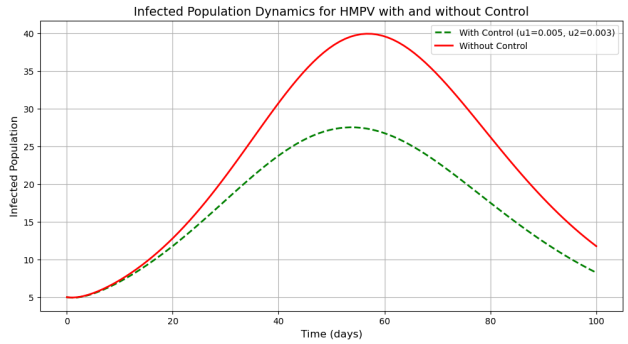

(c) Infected (I)

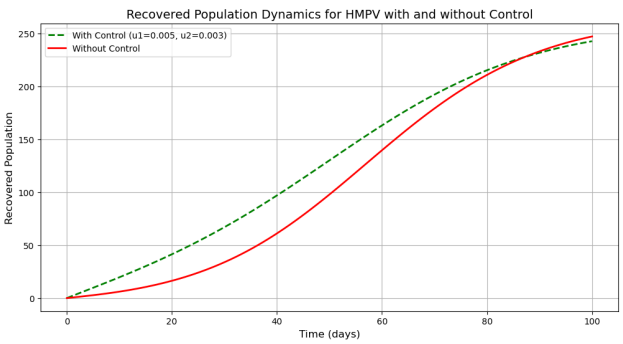

(d) Recovered (R)

Figure 5. Population dynamics for HMPV under Control Strategy A ($u_1 = 0.005, u_2 = 0.003$) compared to the no-control scenario. The curves represent expected trajectories averaged over 500 stochastic realizations.

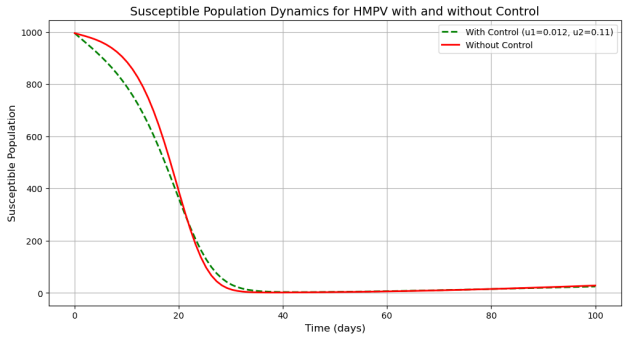

(a) Susceptible (S)

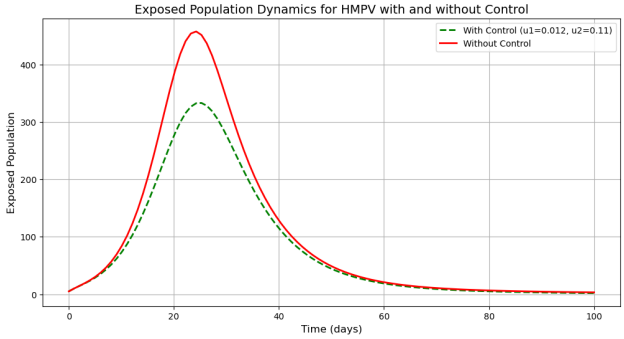

(b) Exposed (E)

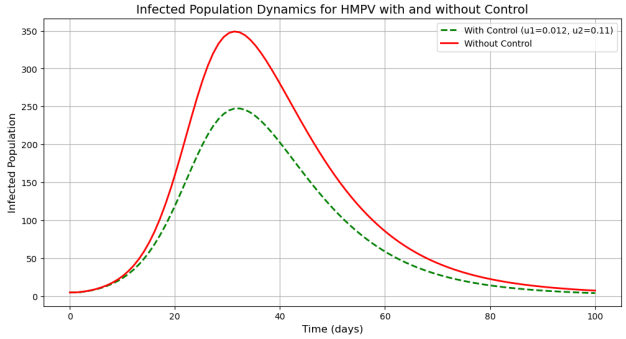

(c) Infected (I)

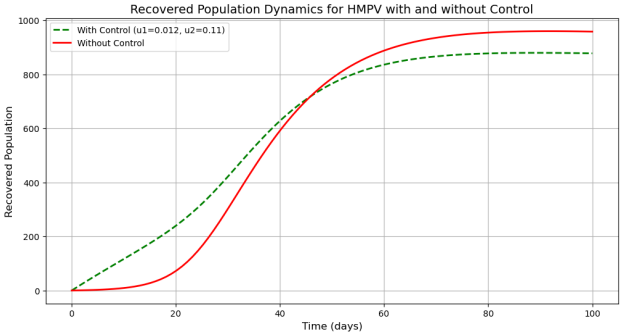

(d) Recovered (R)

Figure 6. Population dynamics for HMPV under Control Strategy B ($u_1 = 0.012, u_2 = 0.11$) compared to the no-control scenario. The curves represent expected trajectories averaged over 500 stochastic realizations.

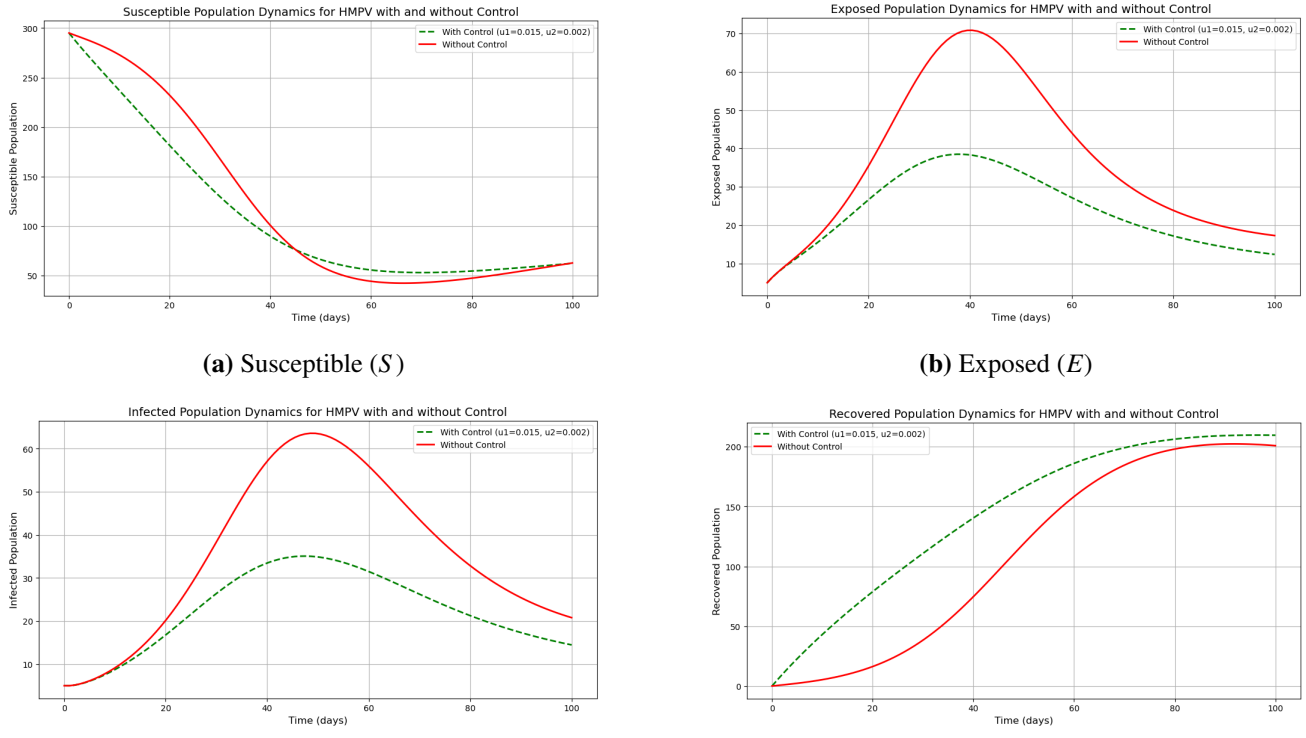

(a) Susceptible (S)

(b) Exposed (E)

(c) Infected (I)

(d) Recovered (R)

Figure 7. Population dynamics for HMPV under Control Strategy C ($u_1 = 0.015, u_2 = 0.002$) compared to the no-control scenario. The curves represent expected trajectories averaged over 500 stochastic realizations.

8. Conclusions

To study the dynamics of HMPV transmission and to improve mitigation strategies, a fractional-order stochastic susceptible-exposed-infected-recovered (SEIR) model was developed in this investigation. The analysis required us to incorporate the effects of memory and environmental stochasticity in the HMPV model framework and subsequently derive a temporally-varying optimal vaccination and therapeutic intervention. The approach combined the Caputo fractional derivatives with the stochastic perturbations that were based on Brownian motion. We thoroughly proved the well-posedness of the system, obtained the basic reproduction number R_0, and performed disease-free equilibrium as well as endemic equilibrium and their local and global stability analyses. It was presented as an optimal control problem and then solved by a numerical solution using a B-spline collocation method. Our significant results approve a forward trans critical bifurcation at the critical threshold $R_0 = 1$, founding this as the precise condition for disease persistence. Our sensitivity analysis concludes that the parameters that exert the most impact the parameters of beta, the parameters of sigma, and the parameters of gamma; thus, these are the main priorities in terms of the intervention. Numerical simulations suggest that treatment-based interventions will decrease peak infection by 36.1% and delay epidemic peaks by 57.8% in response to a reduction in Fractional order; 1.0 is reduced to 0.7. These limitations include homogeneous mixing assumptions, constant population and simplified stochastic formulations. Validation of the model against clinical surveillance

data or outbreak records remains an important next step; our framework provides the mathematical foundation upon which such empirical calibration can be built. Fractional order α encapsulates the intensity of epidemiological memory; its numerical value for a specific outbreak would be determined by fitting the model to empirical incidence data using established parameter estimation techniques for fractional differential equations. From a control perspective, this memory dependence translates into a clear operational principle; when α is lower, interventions should be deployed earlier but need not be as forceful to achieve comparable suppression. The observed linear correlation between α and the optimal intervention peak time provides a quantitative reference for adjusting public health timelines once the memory parameter is estimated. In future studies, researchers need to combine age-structured associates, explore discretetime fractional formulations that align more naturally with surveillance reporting intervals, test the model empirically on region-specific HMPV data, and extend the control paradigm to suit resource constraints and multi-objective optimization. As a result, the given framework provides a rigorous tool in the development of effective adaptive interventions on the population-health level to HMPV outbreaks that consider realistic memory effects and uncertainty.

Author contributions

Md Hossain Islam: Writing original draft, conceptualization, methodolog, software, validation; Md. Nur Alam: Conceptualization, validation, project management, supervision; Noor Muhammad: Conceptualization, methodology, formal analysis, writing original draft, validation, project management; Xinsong Yang: Validation, investigation, review, supervision, project analysis; Md. Jakir Hossen: Formal analysis, supervision, project administration. All authors have read and approved the final version of the manuscript for publication.

Use of Generative-AI tools declaration

The authors declare that they have not used artificial intelligence (AI) tools in the creation of this article.

Acknowledgments

The authors would like to thank the anonymous referees for their valuable comments and suggestions, which led to considerable improvement of the article.

This research did not receive funding.

Conflict of interest

The authors declare that they have no competing interests.

References

1. B. G. Van den Hoogen, J. C. de Jong, J. Groen, T. Kuiken, R. de Groot, R. A. M. Fouchier, et al., A newly discovered human pneumovirus isolated from young children with respiratory tract disease, *Nat. Med.*, **7** (2001), 719–724. https://doi.org/10.1038/89098

2. S. Panda, N. K. Mohakud, L. Pena, S. Kumar, Human metapneumovirus: Review of an important respiratory pathogen, *Int. J. Infect. Dis.*, **25** (2014), 45–52. https://doi.org/10.1016/j.ijid.2014.03.1394
3. K. Mohammadi, S. Faramarzi, S. Yaribash, Z. Valizadeh, E. Rajabi, M. Ghavam, et al. Human metapneumovirus (hMPV) in 2025: Emerging trends and insights from community and hospital-based respiratory panel analyses-a comprehensive review, *Virol. J.*, **22** (2025), 150. https://doi.org/10.1186/s12985-025-02782-y
4. W. Mahikul, L. J. White, K. Poovorawan, N. Soonthornworasiri, P. Sukontamarn, P. Chanthavilay, et al., Modeling household dynamics on respiratory syncytial virus (RSV), *PLoS One*, **14** (2019). https://doi.org/10.1371/journal.pone.0219323
5. A. Sobanjo-ter Meulen, A. V. Gutierrez, O. Ruiz, J. Eeuwijk, H. Vroling, N. Kanesa-Thasan, The burden of human metapneumovirus (hMPV) disease in older and high-risk adults in developed countries: A systematic literature review, *Infect. Dis. Ther.*, **14** (2025), 1917–1933. https://doi.org/10.1007/s40121-025-01187-2
6. W. Cao, J. Xu, F. Zhu, B. Cao, Addressing the unmet needs: Optimized vaccine design for human metapneumovirus, *Innov. Med.*, **3** (2025), 100112. https://doi.org/10.59717/j.xinn-med.2025.100112
7. N. Muhammad, M. N. Alam, Z. Shiqing, Intelligent-based neural networks and optimal control of fractional order Ebola virus dynamics, *arXiv preprint*, 2025.
8. H. W. Hethcote, The mathematics of infectious diseases, *SIAM Rev.*, **42** (2000), 599–653. https://doi.org/10.1137/S0036144500371907
9. N. Muhammad, M. N. Alam, Z. Shiqing, Modeling and analysis of dynamic waveforms in nonlinear fractional models of fifth order, *Comput. Methods Diffe.*, 2025. https://doi.org/10.22034/cmde.2025.68014.3265
10. W. O. Kermack, A. G. McKendrick, A contribution to the mathematical theory of epidemics, *P. Roy. Soc. A*, **115** (1927), 700–721. https://doi.org/10.1098/rspa.1927.0118
11. F. Brauer, P. Driessche, J. H. Wu, *Mathematical epidemiology*, Springer, 2008. https://doi.org/10.1007/978-3-540-78911-6
12. P. Van den Driessche, J. Watmough, Reproduction numbers and subthreshold endemic equilibria for compartmental models of disease transmission, *Math. Biosci.*, **180** (2002), 29–48. https://doi.org/10.1016/S0025-5564(02)00108-6
13. L. J. S. Allen, *An introduction to stochastic epidemic models*, in Mathematical Epidemiology, Springer, 2008, 81–130.
14. M. Wang, P. van den Driessche, L. L. E. Cowen, J. Ma, Distributions of prevalence and daily new cases in a stochastic linear SEIR model, *Math. Biosci.*, **388** (2025), 109508. https://doi.org/10.1016/j.mbs.2025.109508
15. D. Temfack, J. Wyse, Sequential Monte Carlo squared for online inference in stochastic epidemic models, *Epidemics*, **52** (2025). https://doi.org/10.1016/j.epidem.2025.100847
16. W. Xu, H. Liu, C. Qin, Dynamics of nonlinear stochastic SEIR infectious disease model with isolation and latency period, *Symmetry*, **17** (2025), 155. https://doi.org/10.3390/sym17020155

17. Y. Sabbar, A. Zeb, N. Gul, D. Kiouach, S. P. Rajasekar, N. Ullah, et al., Stationary distribution of an SIR epidemic model with three correlated Brownian motions and general Lévy measure, *AIMS Math.*, **8** (2023), 1329–1344. https://doi.org/10.3934/math.2023066

18. A. Gray, D. Greenhalgh, L. Hu, X. Mao, J. Pan, A stochastic differential equation SIS epidemic model, *SIAM J. Appl. Math.*, **71** (2011), 876–902. https://doi.org/10.1137/10081856X

19. J. Du, C. Qin, Y. Hui, Optimal control and analysis of a stochastic SEIR epidemic model with nonlinear incidence and treatment, *AIMS Math.*, **9** (2024), 33532–33550. https://doi.org/10.3934/math.20241600

20. H. M. Wanjala, M. O. Okongo, J. O. Ochwach, Mathematical modelling with optimal control of infectious diseases with vaccination, *Comput. Methods Diffe.*, **14** (2026), 616–632. https://doi.org/10.22034/cmde.2024.62350.2743

21. K. K. Ali, K. Raslsn, A. F. Koura, M. A. Shaalan, Numerical treatment and optimal control of the hepatitis B virus spatio-temporal model, *Comput. Methods Diffe.*, **14** (2026), 95–109.

22. M. S. Hasan, M. N. Alam, M. Fayz-Al-Asad, N. Muhammad, C. Tun, B-spline curve theory: An overview and applications in real life, *Nonlinear Eng.*, **13** (2024), 20240054. https://doi.org/10.1515/nleng-2024-0054

23. M. Qasim, H. Ali, A. Farooq, M. Kamran, H. Ahmad, F. A. Awwad, et al., Intelligent neural framework for modeling the lifestyle-induced remission in the type 2 diabetes, *Chaos Soliton. Fract.*, **205** (2026), 117841. https://doi.org/10.1016/j.chaos.2025.117841

24. L. Tang, H. Wang, X. Zhao, N. Xu, L. Li, Adaptive fixed-time bipartite containment control for saturated nonlinear multi-agent systems based on optimized backstepping technique, *Math. Methods Appl. Sci.*, **205** (2026), 117841. https://doi.org/10.1016/j.chaos.2025.117841

25. C. Chu, Y. He, A unified neural event-triggered control approach of high-order switched uncertain systems with time-varying state constraints, *Robot. Intell. Automat.*, **46** (2026), 290–302. https://doi.org/10.1108/RIA-09-2025-0295

26. S. N. K. A. Khan, M. Y. Misro, Hybrid B-spline collocation method with particle swarm optimization for solving linear differential problems, *AIMS Math.*, **10** (2025), 5399–5420. https://doi.org/10.3934/math.2025249

27. A. Chertock, A. S. Iskhakov, S. Janajra, A. Kurganov, *Spline-based stochastic collocation methods for uncertainty quantification in nonlinear hyperbolic PDEs*, in European Conference on Numerical Mathematics and Advanced Applications, Springer, Cham, 2023, 239–248. https://doi.org/10.1007/978-3-031-86173-4_24

28. J. C. Pedjeu, G. S. Ladde, Stochastic fractional differential equations: Modeling, method and analysis, *Chaos Soliton. Fract.*, **45** (2012), 279–293. https://doi.org/10.1016/j.chaos.2011.12.009

29. H. Zhang, G. Chen, X. Wu, Y. Zhao, Y. Wang, Dynamic analysis of a fractional-order SEAIR model for influenza transmission with optimal control and stochastic stability, *AIMS Math.*, **10** (2025), 20157–20198. https://doi.org/10.3934/math.2025901

30. Z. U. A. Zafar, S. Ijaz, C. Tunc, Numerical analysis of the SEIR epidemic model with fractional order, *Comput. Methods Diffe.*, **14** (2026), 392–410.

31. F. Evirgen, E. Uar, S. Uar, N. zdemir, Modelling influenza a disease dynamics under Caputo-Fabrizio fractional derivative with distinct contact rates, *Math. Model. Numer. Simul. Appl.*, **3** (2023), 58–73. https://doi.org/10.53391/mmnsa.1274004
32. B. G. van den Hoogen, J. C. de Jong, J. Groen, T. Kuiken, R. de Groot, R. A. M. Fouchier, et al., A newly discovered human pneumovirus isolated from young children with respiratory tract disease, *Nat. Med.*, **7** (2001), 719–724. https://doi.org/10.1038/89098
33. N. Muhammad, M. N. Alam, Z. Shiqing, Mathematical modeling and analysis of human metapneumovirus transmission dynamics using neural network intelligence and optimal control, *Comput. Biol. Chem.*, **123** (2026), 109008. https://doi.org/10.1016/j.compbiolchem.2026.109008
34. S. Ghosh, P. J. Birrell, D. De Angelis, An approximate diffusion process for environmental stochasticity in infectious disease transmission modelling, *PLoS Comput. Biol.*, **19** (2023), e1011088. https://doi.org/10.1371/journal.pcbi.1011088
35. E. Tornatore, S. M. Buccellato, P. Vetro, Stability of a stochastic SIR system, *Physica A*, **354** (2005), 111–126. https://doi.org/10.1016/j.physa.2005.02.057
36. D. Matignon, *Stability results for fractional differential equations with applications to control processing*, in Computational Engineering in Systems Applications, Vol. 2, IMACS, IEEE-SMC, Lille, France, 1996, 963–968.
37. Y. Li, Y. Chen, I. Podlubny, Stability of fractional-order nonlinear dynamic systems: Lyapunov direct method and generalized Mittag-Leffler stability, *Comput. Math. Appl.*, **59** (2010), 1810–1821. https://doi.org/10.1016/j.camwa.2009.08.019
38. P. Van den Driessche, J. Watmough, Reproduction numbers and sub-threshold endemic equilibria for compartmental models of disease transmission, *Math. Biosci.*, **180** (2002), 29–48. https://doi.org/10.1016/S0025-5564(02)00108-6
39. K. Diethelm, *The analysis of fractional differential equations: An application-oriented exposition using differential operators of Caputo type*, Springer-Verlag, 2010. https://doi.org/10.1007/978-3-642-14574-2
40. I. Area, J. Losada, J. J. Nieto, A note on the fractional logistic equation, *Physica A*, **444** (2015), 182–187. https://doi.org/10.1016/j.physa.2015.10.037
41. E. Ahmed, A. M. A. El-Sayed, H. A. El-Saka, On some Routh-Hurwitz conditions for fractional order differential equations and their applications in Lorenz, Rssler, Chua and Chen systems, *Phys. Lett. A*, **358** (2006), 1–4. https://doi.org/10.1016/j.physleta.2006.04.087
42. N. Aguila-Camacho, M. A. Duarte-Mermoud, J. A. Gallegos, Lyapunov functions for fractional order systems, *Commun. Nonlinear Sci.*, **19** (2014), 2951–2957. https://doi.org/10.1016/j.cnsns.2014.01.022
43. J. Carr, *Applications of centre manifold theory*, Springer Science & Business Media, **35** (2012).
44. C. Castillo-Chavez, B. Song, Dynamical models of tuberculosis and their applications, *Math. Biosci. Eng.*, **1** (2004), 361–404. https://doi.org/10.3934/mbe.2004.1.361
45. S. Marino, I. B. Hogue, C. J. Ray, D. E. Kirschner, A methodology for performing global uncertainty and sensitivity analysis in systems biology, *J. Theor. Biol.*, **254** (2008), 178–196. https://doi.org/10.1016/j.jtbi.2008.04.011

46. A. A. Kilbas, H. M. Srivastava, J. J. Trujillo, *Theory and applications of fractional differential equations*, Elsevier, **204** (2006).

47. B. Mezerdi, S. Bahlali, Necessary conditions for optimality in relaxed stochastic control problems, *Stochastics*, **73** (2002), 201–218. https://doi.org/10.1080/1045112021000025925

48. Y. S. Mishura, *Stochastic calculus for fractional Brownian motion and related processes*, Springer Science & Business Media, 2008. https://doi.org/10.1007/978-3-540-75873-0

49. C. Sorgentone, E. Pellegrino, F. Pitolli, A spline-based framework for solving the space-time fractional convection-diffusion problem, *Appl. Math. Lett.*, **161** (2025), 109370. https://doi.org/10.1016/j.aml.2024.109370

50. S. Malge, R. K. Lodhi, Quintic B-spline method for numerical solution of second-order singularly perturbed delay differential equations, *Comput. Methods Diffe.*, **14** (2026), 36–49.

51. M. S. Arif, K. Abodayeh, Y. Nawaz, Precision in disease dynamics: Finite difference solutions for stochastic epidemics with treatment cure and partial immunity, *Part. Differ. Equ. Appl. Math.*, **9** (2024), 100660. https://doi.org/10.1016/j.padiff.2024.100660

AIMS Press